(12) INTERNATIONAL APPLICATION PUBLISHED UNDER THE PATENT COOPERATION TREATY (PCT)

(19) World Intellectual Property Organization
International Bureau

(43) International Publication Date
20 January 2022 (20.01.2022)

WIPO | PCT

(10) International Publication Number
WO 2022/013256 A1

(51) International Patent Classification:
G01N 33/574 (2006.01)

(21) International Application Number:
PCT/EP2021/069529

(22) International Filing Date:
13 July 2021 (13.07.2021)

(25) Filing Language: English

(26) Publication Language: English

(30) Priority Data:
20305811.0 15 July 2020 (15.07.2020) EP

(71) Applicants: **INSERM (INSTITUT NATIONAL DE LA SANTÉ ET DE LA RECHERCHE MÉDICALE)** [FR/FR]; 101, rue de Tolbiac, 75013 Paris (FR). **UNIVERSITÉ D'AIX MARSEILLE** [FR/FR]; 58 Boulevard Charles Livon, 13284 Marseille Cedex 07 (FR). **ASSISTANCE PUBLIQUE HÔPITAUX DE MARSEILLE** [FR/FR]; 80 Rue Brochier, 13005 Marseille (FR). **CENTRE NATIONAL DE LA RECHERCHE SCIENTIFIQUE (CNRS)** [FR/FR]; 3, Rue Michel Ange, 75016 Paris (FR). **INNATE PHARMA** [FR/FR]; 117, avenue de Luminy, 13009 MARSEILLE (FR).

(72) Inventors: **VIVIER, Eric**; Aix Marseille Université - INSERM - CNRS Campus de Luminy, Case 906, 13288 MARSEILLE Cedex 09 (FR). **NARNI-MANCINELLI, Emilie**; CENTRE D'IMMUNOLOGIE DE MARSEILLE - LUMINY (CIML) - U1104 163 AVENUE DE LUMINY - Campus de Luminy, Case 906, 13288 MARSEILLE CEDEX 9 (FR). **ESCALIERE, Bertrand**; CENTRE D'IMMUNOLOGIE DE MARSEILLE - LUMINY (CIML) - U1104 163 AVENUE DE LUMINY - Campus de Luminy, Case 906, 13288 MARSEILLE CEDEX 9 (FR). **DUMAS, Pierre Yves**; CENTRE D'IMMUNOLOGIE DE MARSEILLE - LUMINY (CIML) - U1104 163 AVENUE DE LUMINY - Campus de Luminy, Case 906, 13288 MARSEILLE CEDEX 9 (FR). **CRINIER, Adeline**; CENTRE D'IMMUNOLOGIE DE MARSEILLE - LUMINY (CIML) - U1104 163 AVENUE DE LUMINY - Campus de Luminy, Case 906, 13288 MARSEILLE CEDEX 9 (FR).

(74) Agent: **INSERM TRANSFERT**; 7 rue Watt, 75013 Paris (FR).

(81) Designated States *(unless otherwise indicated, for every kind of national protection available)*: AE, AG, AL, AM, AO, AT, AU, AZ, BA, BB, BG, BH, BN, BR, BW, BY, BZ, CA, CH, CL, CN, CO, CR, CU, CZ, DE, DJ, DK, DM, DO, DZ, EC, EE, EG, ES, FI, GB, GD, GE, GH, GM, GT, HN, HR, HU, ID, IL, IN, IR, IS, IT, JO, JP, KE, KG, KH, KN, KP, KR, KW, KZ, LA, LC, LK, LR, LS, LU, LY, MA, MD, ME, MG, MK, MN, MW, MX, MY, MZ, NA, NG, NI, NO, NZ, OM, PA, PE, PG, PH, PL, PT, QA, RO, RS, RU, RW, SA, SC, SD, SE, SG, SK, SL, ST, SV, SY, TH, TJ, TM, TN, TR, TT, TZ, UA, UG, US, UZ, VC, VN, WS, ZA, ZM, ZW.

(84) Designated States *(unless otherwise indicated, for every kind of regional protection available)*: ARIPO (BW, GH, GM, KE, LR, LS, MW, MZ, NA, RW, SD, SL, ST, SZ, TZ, UG, ZM, ZW), Eurasian (AM, AZ, BY, KG, KZ, RU, TJ, TM), European (AL, AT, BE, BG, CH, CY, CZ, DE, DK, EE, ES, FI, FR, GB, GR, HR, HU, IE, IS, IT, LT, LU, LV, MC, MK, MT, NL, NO, PL, PT, RO, RS, SE, SI, SK, SM, TR), OAPI (BF, BJ, CF, CG, CI, CM, GA, GN, GQ, GW, KM, ML, MR, NE, SN, TD, TG).

Published:
— *with international search report (Art. 21(3))*
— *with sequence listing part of description (Rule 5.2(a))*

WO 2022/013256 A1

(54) Title: USE OF CD160 AS A BIOMARKER IN ACUTE MYELOID LEUKEMIA

(57) Abstract: Natural killer (NK) cells are innate cytotoxic lymphoid cells (ILCs) involved in the killing of infected and tumor cells. Several NK cell subsets have been reported in humans, but their heterogeneity between tissues remains to be fully characterized. The inventors previously showed, by single-cell RNA sequencing (scRNAseq) in human and mouse NK cells from spleen and blood, that the two major subsets, NK1 and NK2, are similar in different organs and species. They report here the identification, at single-cell resolution, of three subpopulations of NK cells in human bone marrow and an additional adaptive cell-like NK population in some cytomegalovirus-seropositive individuals. Pseudotime analysis identified a minor subset of resident CD56 bright NK cells, NK0 cells, as the precursor of both circulating CD56 dim NK1-like NK cells and CD56 bright NK2-like in the human bone marrow and spleen at steady state. Transcriptomic profiles of bone marrow NK cells from patients with acute myeloid leukemia (AML), a bone marrow disease, showed a stress-induced repression of NK cell effector functions relative to healthy NK cells, thus highlighting the profound impact of the disease on NK cell heterogeneity. Finally, the inventors investigated the potential role of CD160 in AML disease development and progression further, by studying the clinical outcome of cancer patients. Survival was much higher in patients with CD160-high AML than in those with CD160-low cancer, suggesting that CD160 is an anti-tumor biomarker in AML.

USE OF CD160 AS A BIOMARKER IN ACUTE MYELOID LEUKEMIA

FIELD OF THE INVENTION:

The present invention is in the field of medicine, in particular oncology.

BACKGROUND OF THE INVENTION:

Natural killer (NK) cells are large granular lymphocytes from the ILC family. NK cells are endowed with a capacity to kill stressed cells, such as infected cells and tumor cells, without specific prior activation, in humans and mice (Vivier et al., 2011). NK cells express an array of inhibitory and activating receptors, the engagement of which regulates NK cell activation. Inhibitory receptors are essential for sensing decreases or total absences of constitutively expressed MHC-I self-molecules on target cells. Decreases in MHC-I expression reduce the strength of the inhibitory signals delivered to NK cells, rendering them more prone to activation (Moretta et al., 2001; Narni-Mancinelli et al., 2013). NK cell activation results from the engagement of activating receptors, such as the activating isoforms of Ly49 and KIRs, the natural cytotoxicity receptors (NCRs), the SLAM (signaling lymphocyte activating molecule)-related receptors, NKG2D and CD16, which can induce NK cell activation by initiating different signaling pathways (Guia et al., 2018). The NCR family is composed of three molecules: NKp30 (NCR3, CD337) and NKp44 (NCR2, CD336) in humans and NKp46 (NCR1, CD335), which is expressed in all mammals and is highly conserved between humans and mice. NKp46 is expressed mostly by NK cells and ILC1, but is also present on a small population of T lymphocytes and a subset of ILC3 (NCR^+ILC3) in mucosa (Spits et al., 2013; Walzer et al., 2007b; Yu et al., 2011).

NK cells are present in the blood, and in primary and secondary lymphoid organs, including the spleen, bone marrow, liver, lymph nodes, lungs, tonsils, skin, uterus, and gut (Bjorkstrom et al., 2016). The NK cell compartment consists of several subsets differing in terms of maturation status. Human NK cells are defined as $CD3^-$ $CD14^-$ $CD19^-$ $CD56^+$ lymphocytes. They can be classified into subsets on the basis of the intensity of cell surface CD56 expression. Two principal NK cell subsets are found in the bloodstream in healthy individuals: $CD56^{dim}$ $CD16^+$ NK cells and $CD56^{bright}$ $CD16^-$ NK cells (Cooper et al., 2001; Hanna et al., 2004; Yu et al., 2013). The phenotypic differences between these cells are associated with functional differences: $CD56^{bright}$ $CD16^-$ NK cells are less cytotoxic than $CD56^{dim}$ $CD16^+$ cells, but

produce larger amounts of cytokines in response to exposure to environmental factors, such as interleukin (IL)-12 and IL-18 (Cooper et al., 2001). We recently used high-throughput scRNAseq to investigate the heterogeneity of the NK cell compartment in the blood and spleen of humans and mice (Crinier et al., 2018). We identified two subsets conserved in human and mouse blood and spleen: NK1 and NK2 cells. In humans, the $CD56^{dim}$ NK1 subset had high levels of cytotoxic activity, whereas $CD56^{bright}$ NK2 cells were enriched in gene ontology (GO) terms relating to the secretion of cytokines and chemokines, consistent with previous findings. We also found two tissue-specific human NK subsets resident in the spleen, which we named hNK_Sp3 and hNK_Sp4. The hNK_Sp3 cells resembled $CD56^{bright}$ NK2 cells, whereas hNK_Sp4 cells seemed to be more mature and more closely resembled the NK1 subset.

Several studies have suggested that $CD56^{bright}$ $CD16^{-}$ cells can develop into $CD56^{dim}$ $CD16^{+}$ NK cells. Indeed, $CD56^{bright}$ NK cells constitute the main NK cell population shortly after hematopoietic stem cell transplantation, subsequently disappearing as $CD56^{dim}$ cell levels rise, three months after transplantation (Dulphy et al., 2008). Purified $CD56^{bright}$ NK cells cocultured *in vitro* with synovial fibroblasts display a downregulation of CD56 and a phenotype consistent with $CD56^{dim}$ NK cells (Chan et al., 2007). *In vivo*, the adoptive transfer of $CD56^{bright}$ NK cells into immunodeficient NOD-SCID recipient mice leads to a $CD56^{dim}CD16^{+}$ phenotype 10 days later, in the blood, spleen, and lymph nodes (Chan et al., 2007). Finally, $CD56^{bright}$ NK cells have been shown to have longer telomere repeats than $CD56^{dim}$ NK cells, suggesting that they are less mature than $CD56^{dim}$ NK cells (Chan et al., 2007).

In both humans and mice, the expansion of a particular population of NK cells, known as "adaptive NK" or "memory NK" cells, has been described during cytomegalovirus (CMV) infection (Lopez-Verges et al., 2011). These adaptive NK cells persist long after the contraction of the anti-CMV immune response and are capable of more powerful effector functions upon reinfection. Adaptive NK cells have also been described following the activation of NK cells by cytokines (Cooper et al., 2009) or exposure to hantavirus infection (Bjorkstrom et al., 2011), herpes simplex virus 2 (HSV-2) (Abdul-Careem et al., 2012) or influenza vaccination in humans (Dou et al., 2015). Adaptive NK cells express the cell surface activating receptor NKG2C in humans, and the maturation marker CD57, and they lack many transcriptional factors and signaling proteins, including FCRγ, PLZF, Siglec-7, EAT-2 and SYK (Cichocki et al., 2016; Lee et al., 2015; Tesi et al., 2016).

Acute myeloid leukemia (AML) is a hematological malignancy characterized by proliferative, clonal immature myeloid cells invading the bone marrow (Short et al., 2020). Blast cells replace normal hematopoiesis and make use of the normal bone marrow microenvironment to survive and to support disease expansion, also affecting immune cells. NK cells from AML patients display low levels of cell surface NCR expression associated with impaired cytotoxicity (Costello et al., 2002; Fauriat et al., 2007). Conversely, high levels of NKp30 and NKp46 on the cell surface have been linked to better outcomes (Chretien et al., 2017a; Chretien et al., 2017c). The downregulation of other activating receptors, including DNAM-1, NKG2C and 2B4 (Chretien et al., 2017b; Pende et al., 2005; Sanchez-Correa et al., 2012), and the upregulation of inhibitory receptors, such as NKG2A (Chretien et al., 2017b; Stringaris et al., 2014), at the surface of NK cells from AML patients, also contribute to the low cytotoxicity and levels of IFN-γ secretion of these cells (Chiossone et al., 2018).

SUMMARY OF THE INVENTION:

As defined by the claims, the present invention relates to the use of CD160 as a biomarker in acute myeloid leukemia.

DETAILED DESCRIPTION OF THE INVENTION:

Natural killer (NK) cells are innate cytotoxic lymphoid cells (ILCs) involved in the killing of infected and tumor cells. Several NK cell subsets have been reported in humans, but their heterogeneity between tissues remains to be fully characterized. The inventors previously showed, by single-cell RNA sequencing (scRNAseq) in human and mouse NK cells from spleen and blood, that the two major subsets, NK1 and NK2, are similar in different organs and species. They report here the identification, at single-cell resolution, of three subpopulations of NK cells in human bone marrow and an additional adaptive cell-like NK population in some cytomegalovirus-seropositive individuals. Pseudotime analysis identified a minor subset of resident $CD56^{bright}$ NK cells, NK0 cells, as the precursor of both circulating $CD56^{dim}$ NK1-like NK cells and $CD56^{bright}$ NK2-like in the human bone marrow and spleen at steady state. Transcriptomic profiles of bone marrow NK cells from patients with acute myeloid leukemia (AML), a bone marrow disease, showed a stress-induced repression of NK cell effector functions relative to healthy NK cells, thus highlighting the profound impact of the disease on NK cell heterogeneity. Finally, the inventors investigated the potential role of CD160 in AML disease development and progression further, by studying the clinical outcome of cancer

patients. Survival was much higher in patients with CD160-high AML than in those with CD160-low cancer, suggesting that CD160 is an anti-tumor biomarker in AML.

Accordingly, the first object of the present invention relates to a method of predicting the survival time of a patient suffering from an acute myeloid leukemia (AML) comprising determining the level of CD160 in a sample obtained from the patient wherein said level correlates with the patient's survival time.

As used herein, the term "**acute myeloid leukemia**" or "**acute myelogenous leukemia**" ("**AML**") refers to a cancer of the myeloid line of blood cells, characterized by the rapid growth of abnormal white blood cells that accumulate in the bone marrow and interfere with the production of normal blood cells.

The method of the present invention is particularly suitable for predicting the duration of the overall survival (OS), progression-free survival (PFS) and/or the disease-free survival (DFS) of the cancer patient. Those of skill in the art will recognize that OS survival time is generally based on and expressed as the percentage of people who survive a certain type of cancer for a specific amount of time. Cancer statistics often use an overall five-year survival rate. In general, OS rates do not specify whether cancer survivors are still undergoing treatment at five years or if they've become cancer-free (achieved remission). DSF gives more specific information and is the number of people with a particular cancer who achieve remission. Also, progression-free survival (PFS) rates (the number of people who still have cancer, but their disease does not progress) includes people who may have had some success with treatment, but the cancer has not disappeared completely.

As used herein, the expression "**short survival time**" indicates that the patient will have a survival time that will be lower than the median (or mean) observed in the general population of patients suffering from said cancer. When the patient will have a short survival time, it is meant that the patient will have a "**poor prognosis**". Inversely, the expression "**long survival time**" indicates that the patient will have a survival time that will be higher than the median (or mean) observed in the general population of patients suffering from said cancer. When the patient will have a long survival time, it is meant that the patient will have a "**good prognosis**".

As used herein, the term "**CD160**" has its general meaning in the art and refers to CD160 molecule. CD160 gene was found to be located on human chromosome 1, and the corresponding protein was originally characterized as a glycosylphosphatidylinositol (GPI)-anchored cell surface molecule. Three CD160 isoforms exist: the CD160-TM isoform, the CD160 GPI-anchored isoform and the soluble CD160 isoform. CD160-GPI is expressed by intestinal intraepithelial T lymphocytes and by a minor subset of circulating lymphocytes including NK cells, TCR$\gamma\delta$ and cytotoxic effector $CD8^{bright}CD28^{-}$ T lymphocytes (ANUMANTHAN et al., 1998, J Immunol; 161:2780-2790; MAIZA et al., J. Exp. Med., vol. 178, p: 1121-1126, 1993). The CD160 transmembrane isoform ("CD160-TM") is described in Giustiniani J et al. (J Immunol. 2009 Jan 1;182(1):63-71.) as well as in the international patent application WO2008155363 and is characterized by the amino acid sequence as set forth in SEQ ID NO: 1. The extracellular domain of the CD160-TM isoform may be defined by the amino acid sequence ranging from the amino acid residue at position 26 to the amino acid residue at position 189 in SEQ ID NO: 1. The CD160 GPI-anchored isoform ("CD160-GPI") is described in Nikolova M. et al. (Int Immunol. 2002 May;14(5):445-51.) as well as in the international patent application WO2006015886 and is characterized by the amino acid sequence as set forth in SEQ ID NO: 2 fused to a GPI anchor at the C terminus end. The CD160 soluble isoform is described in Giustiniani J. et al. (J Immunol. 2007 Feb 1;178(3):1293-300) and is characterized by the amino acid sequence as set forth in SEQ ID NO: 3. In SEQ ID NO: 1-3, amino acids 1-25 correspond to a signal peptide, and may consequently be absent from the expressed protein.

SEQ ID NO: 1: CD160-TM isoform
MLLEPGRGCCALAILLAIVDIQSGGCINITSSASQEGTRLNLICTVWHKKEEAEGFVVFLCKDRSGDCSPETSLK
QLRLKRDPGIDGVGEISSQLMFTISQVTPLHSGTYQCCARSQKSGIRLQGHFFSILFTETGNYTVTGLKQRQHLE
FSHNEGTLSSGFLQEKVWVMLVTSLVALQGMSKRAVSTPSNEGAIIFLPPWLFSRRRRLERMSRGREKCYSSPGY
PQESSNQFH
SEQ ID NO: 2 CD160 GPI-anchored isoform
MLLEPGRGCCALAILLAIVDIQSGGCINITSSASQEGTRLNLICTVWHKKEEAEGFVVFLCKDRSGDCSPETSLK
QLRLKRDPGIDGVGEISSQLMFTISQVTPLHSGTYQCCARSQKSGIRLQGHFFSILFTETGNYTVTGLKQRQHLE
FSHNEGTLSS
SEQ ID NO: 3: CD160 soluble isoform
MLLEPGRGCCALAILLAIVDIQSGGCINITSSASQEGTRLNLICTVWHKKEEAEGFVVFLCKDRSGDCSPETSLK
QLRLKRDPGIDGVGEISSQLMFTISQVTPLHSGTYQCCARSQKSGIRLQGHFFSILFTETGNYTVTGLKQRQHLE
FSHNEGTLSS

As used herein, the term "**sample**" refers to any sample obtained from the subject for the purpose of performing the method of the present invention. In some embodiments, the sample is a bodily fluid (e.g. a blood sample), a population of cells, or a tissue. Typically the sample is obtained at AML diagnosis.

In some embodiments, the sample is a blood sample. As used herein, the term "**blood sample**" refers to a whole blood sample, serum sample and plasma sample. A blood sample may be obtained by methods known in the art including venipuncture or a finger stick. Serum and plasma samples may be obtained by centrifugation methods known in the art. The sample may be diluted with a suitable buffer before conducting the assay. In some embodiments, the sample is a PBMC sample. The term "**PBMC**" or "**peripheral blood mononuclear cells**" or "**unfractionated PBMC**", as used herein, refers to whole PBMC, i.e. to a population of white blood cells having a round nucleus, which has not been enriched for a given sub-population. Cord blood mononuclear cells are further included in this definition. Typically, the PBMC sample according to the invention has not been subjected to a selection step to contain only adherent PBMC (which consist essentially of >90% monocytes) or non-adherent PBMC. A PBMC sample according to the invention therefore contains lymphocytes (B cells, T cells, ILCs cells, and NKT cells), monocytes, and precursors thereof. Typically, these cells can be extracted from whole blood using Ficoll, a hydrophilic polysaccharide that separates layers of blood, with the PBMC forming a cell ring under a layer of plasma. Additionally, PBMC can be extracted from whole blood using a hypotonic lysis buffer which will preferentially lyse red blood cells. Such procedures are known to the expert in the art.

In some embodiments, the sample is a bone marrow sample.

As used herein, the term "**bone marrow sample**" has its general in the art and refers to material pulled out the bone marrow cavity by suction, which includes, but is not limited to, bone marrow aspiration and bone marrow biopsy. In some embodiments, the bone marrow sample results from a biopsy performed in the bone marrow of the patient. The bone marrow sample can, of course, be subjected to a variety of well-known post-collection preparative and storage techniques (e.g., fixation, storage, freezing, etc.). The sample can be fresh, frozen, fixed (e.g., formalin fixed), or embedded (e.g., paraffin embedded).

In some embodiments, the level of CD160 is determined at the protein level by any well-known method in the art. Typically, such methods comprise contacting the sample with at least one selective binding agent capable of selectively interacting with CD160. The selective binding agent may be polyclonal antibody or monoclonal antibody, an antibody fragment, synthetic antibodies, or other protein-specific agents such as nucleic acid or peptide aptamers. For the detection of the antibody that makes the presence of the marker detectable by microscopy or an automated analysis system, the antibodies may be tagged directly with detectable labels such as enzymes, chromogens or fluorescent probes or indirectly detected with a secondary antibody conjugated with detectable labels. In some embodiments, sample, the level of the marker is determined by immunohistochemistry (IHC). Immunohistochemistry typically includes the following steps i) fixing said sample with formalin, ii) embedding said sample in paraffin, iii) cutting said sample into sections for staining, iv) incubating said sections with the binding partner specific for the marker, v) rinsing said sections, vi) incubating said section with a biotinylated secondary antibody and vii) revealing the antigen-antibody complex with avidin-biotin-peroxidase complex. Accordingly, the sample is firstly incubated the binding partners. After washing, the labeled antibodies that are bound to marker of interest are revealed by the appropriate technique, depending of the kind of label is borne by the labeled antibody, e.g. radioactive, fluorescent or enzyme label. Multiple labelling can be performed simultaneously. Alternatively, the method of the present invention may use a secondary antibody coupled to an amplification system (to intensify staining signal) and enzymatic molecules. Such coupled secondary antibodies are commercially available, e.g. from Dako, EnVision system. Counterstaining may be used, e.g. H&E, DAPI, Hoechst. Other staining methods may be accomplished using any suitable method or system as would be apparent to one of skill in the art, including automated, semi-automated or manual systems.

In some embodiments, the level of CD160 is determined at nucleic acid level. Typically, the level of CD160 may be determined by determining the quantity of mRNA encoding for CD160. Methods for determining the quantity of mRNA are well known in the art. For example, the nucleic acid contained in the samples (e.g., cell or tissue prepared from the subject) is first extracted according to standard methods, for example using lytic enzymes or chemical solutions or extracted by nucleic-acid-binding resins following the manufacturer's instructions. The extracted mRNA is then detected by hybridization (e. g., Northern blot analysis, in situ hybridization) and/or amplification (e.g., RT-PCR). Other methods of Amplification include ligase chain reaction (LCR), transcription-mediated amplification (TMA), strand displacement

amplification (SDA), nucleic acid sequence based amplification (NASBA), ISH procedures (for example, fluorescence in situ hybridization (FISH), chromogenic in situ hybridization (CISH) and silver in situ hybridization (SISH)) or comparative genomic hybridization (CGH). In some embodiments, the level of CD160 mRNA is quantified by nCounter® analysis (Nanostring, USA). In some embodiments, the level of CD160 mRNA is quantified by sequencing (RNA sequencing). In some embodiments, the level of CD160 mRNA is quantified by nucleic acid array (e.g. microarrays).

As used herein, the term "**NK cells**" or "**natural killer cells**" has its general meaning in the art and refers to innate cytotoxic lymphoid cells (ILCs) involved in the killing of infected and tumor cells. NK cells can be identified by virtue of certain characteristics and biological properties. Typically, human NK cells are Lin- CD56+ lymphocytes, with a lineage including necessary CD3, and sometimes other markers such as CD14 and/or CD19 for example without being limited to the inclusion of these two. In some embodiments, the NK cells are defined as CD3- CD14- CD19- CD56+ lymphocytes.

In some embodiments, the level of CD160 is expressed as measurement of the expression intensity of the marker (e.g. protein and/or mRNA) by NK cells (e.g. mean fluorescence intensity MFI) or as measurement of the amount of NK cells that express CD160 (e.g. protein and/or mRNA) in a sample (e.g. frequencies (e.g. %) of CD160+ NK cells and density of C160+ NK cells).

Methods for quantifying expression level of CD160 in NK cells in a sample are well known in the art and typically involve the presence or absence of specific cell surface markers. In some embodiments, determining the presence or absence of the cell surface markers involves use of a panel of binding partners specific for the cell surface markers of interest. Said binding partners include but are not limited to antibodies, aptamer, and peptides. The binding partners will allow for the screening of cellular populations expressing the marker. Various techniques can be utilized to screen for cellular populations expressing the cell surface markers of interest, and typically include magnetic separation using antibody-coated magnetic beads, "panning" with antibody attached to a solid matrix (i.e., plate), and flow cytometry (See, e.g., U.S. Pat. No. 5,985,660; and Morrison et al. Cell, 96:737-49 (1999)).

In some embodiments, the binding partners are antibodies that may be polyclonal or monoclonal, preferably monoclonal, specifically directed against one cell surface marker. Polyclonal antibodies of the invention or a fragment thereof can be raised according to known methods by administering the appropriate antigen or epitope to a host animal selected, e.g., from pigs, cows, horses, rabbits, goats, sheep, and mice, among others. Various adjuvants known in the art can be used to enhance antibody production. Although antibodies useful in practicing the invention can be polyclonal, monoclonal antibodies are preferred. Monoclonal antibodies of the invention or a fragment thereof can be prepared and isolated using any technique that provides for the production of antibody molecules by continuous cell lines in culture. Techniques for production and isolation include but are not limited to the hybridoma technique originally; the human B-cell hybridoma technique; and the EBV-hybridoma technique.

In some embodiments, the panel of binding partners that are specific for the following cell surface markers CD3, CD56 and CD160 can be used.

Typically, the binding partners are conjugated with a label for use in separation. Labels include magnetic beads, which allow for direct separation, biotin, which can be removed with avidin or streptavidin bound to a support, fluorochromes, which can be used with a fluorescence activated cell sorter, or the like, to allow for ease of separation of the particular cell type. Fluorochromes that find use include phycobiliproteins, e.g. phycoerythrin and allophycocyanins, fluorescein and Texas red. Typically each antibody is labeled with a different fluorochrome, to permit independent sorting for each marker. Suitable fluorescent detection elements include, but are not limited to, fluorescein, rhodamine, tetramethylrhodamine, eosin, erythrosin, coumarin, methyl-coumarins, pyrene, Malacite green, stilbene, Lucifer Yellow, Cascade Blue™, Texas Red, IAEDANS, EDANS, BODIPY FL, LC Red 640, Cy 5, Cy 5.5, LC Red 705 and Oregon green. Suitable optical dyes are described in the 1996 Molecular Probes Handbook by Richard P. Haugland, hereby expressly incorporated by reference. Suitable fluorescent labels also include, but are not limited to, green fluorescent protein (GFP; Chalfie, et al., Science 263(5148):802-805 (Feb. 11, 1994); and EGFP; Clontech—Genbank Accession Number U55762), blue fluorescent protein (BFP; 1. Quantum Biotechnologies, Inc. 1801 de Maisonneuve Blvd. West, 8th Floor, Montreal (Quebec) Canada H3H 1J9; 2. Stauber, R. H. Biotechniques 24(3):462-471 (1998); 3. Heim, R. and Tsien, R. Y. Curr. Biol. 6:178-182 (1996)), enhanced yellow fluorescent protein (EYFP; 1. Clontech Laboratories, Inc., 1020 East

Meadow Circle, Palo Alto, Calif. 94303), luciferase (Ichiki, et al., J. Immunol. 150(12):5408-5417 (1993)), (β-galactosidase (Nolan, et al., Proc Natl Acad Sci USA 85(8):2603-2607 (April 1988)) and Renilla WO 92/15673; WO 95/07463; WO 98/14605; WO 98/26277; WO 99/49019; U.S. Pat. Nos. 5,292,658; 5,418,155; 5,683,888; 5,741,668; 5,777,079; 5,804,387; 5,874,304; 5,876,995; and 5,925,558). All of the above-cited references are expressly incorporated herein by reference. In some embodiments, detection elements for use in the present invention include: Alexa-Fluor dyes (an exemplary list including Alexa Fluor® 350, Alexa Fluor® 405, Alexa Fluor® 430, Alexa Fluor® 488, Alexa Fluor® 500, Alexa Fluor® 514,Alexa Fluor® 532, Alexa Fluor® 546, Alexa Fluor® 555, Alexa Fluor® 568, Alexa Fluor® 594, Alexa Fluor® 610, AlexaFluor® 633, Alexa Fluor® 647, Alexa Fluor® 660, Alexa Fluor® 680, Alexa Fluor® 700, and Alexa Fluor® 750), Cascade Blue, Cascade Yellow and R-phycoerythrin (PE) (Molecular Probes) (Eugene, Oreg.), FITC, Rhodamine, and Texas Red (Pierce, Rockford, Ill.), Cy5, Cy5.5, Cy7 (Amersham Life Science, Pittsburgh, Pa.). Tandem conjugate protocols for Cy5PE, Cy5.5PE, Cy7PE, Cy5.5APC, Cy7APC are known in the art. Fluorophores bound to antibody or other binding element can be activated by a laser and re-emit light of a different wavelength. The amount of light detected from the fluorophores is related to the number of binding element targets associated with the cell passing through the beam. Any specific set of detection elements, e.g. fluorescently tagged antibodies, in any embodiment can depend on the types of cells to be studied and the presence of the activatable element within those cells. Several detection elements, e.g. fluorophore-conjugated antibodies, can be used simultaneously, so measurements made as one cell passes through the laser beam consist of scattered light intensities as well as light intensities from each of the fluorophores. Thus, the characterization of a single cell can consist of a set of measured light intensities that may be represented as a coordinate position in a multi-dimensional space. Considering only the light from the fluorophores, there is one coordinate axis corresponding to each of the detection elements, e.g. fluorescently tagged antibodies. The number of coordinate axes (the dimension of the space) is the number of fluorophores used. Modern flowcytometers can measure several colors associated with different fluorophores and thousands of cells per second. Thus, the data from one subject can be described by a collection of measurements related to the number of antigens for each of (typically) many thousands of individual cells. See Krutzik et al., High-content single-cell drug screening with phosphospecific flow cytometry. Nature Chemical Biology, Vol. 4 No. 2, Pgs. 132-42, February 2008. Such methods may optionally include the use of barcoding to increase throughput and reduce consumable consumption. See Krutzik, P.

and Nolan, G., Fluorescent cell barcoding in flow cytometry allows high-throughput drug screening and signaling profiling. Nature Methods, Vol. 3 No. 5, Pgs. 361-68, May 2006.

Thus in some embodiments, the quantification of CD160 on NK cells is carried out by a flow cytometric method. As used herein, the term "**flow cytometric method**" refers to a technique for counting cells of interest, by suspending them in a stream of fluid and passing them through an electronic detection apparatus. Flow cytometric methods allow simultaneous multiparametric analysis of the physical and/or chemical parameters of up to thousands of events per second, such as fluorescent parameters. Modern flow cytometric instruments usually have multiple lasers and fluorescence detectors. A common variation of flow cytometric techniques is to physically sort particles based on their properties, so as to purify or detect populations of interest, using "fluorescence-activated cell sorting". As used herein, "**fluorescence-activated cell sorting**" or "**FACS**" refers to a flow cytometric method for sorting a heterogeneous mixture of cells from a biological sample into two or more containers, one cell at a time, based upon the specific light scattering and fluorescent characteristics of each cell and provides fast, objective and quantitative recording of fluorescent signals from individual cells as well as physical separation of cells of particular interest. Accordingly, FACS can be used with the methods described herein to isolate and detect the population of cells of the present invention. For example, fluorescence activated cell sorting (FACS) may be therefore used and typically involves a flow cytometer capable of simultaneous excitation and detection of multiple fluorophores, such as a BD Biosciences FACSCanto™ flow cytometer, used substantially according to the manufacturer's instructions. The cytometric systems may include a cytometric sample fluidic subsystem, as described below. In addition, the cytometric systems include a cytometer fluidically coupled to the cytometric sample fluidic subsystem. Systems of the present disclosure may include a number of additional components, such as data output devices, e.g., monitors, printers, and/or speakers, softwares (e.g. (Flowjo, Laluza....), data input devices, e.g., interface ports, a mouse, a keyboard, etc., fluid handling components, power sources, etc. More particularly, the sample is contacted with a panel of antibodies specific for the specific market of the population of cells of the interest.

In some embodiments the binding partner is conjugated to a metallic chemical element such as lanthanides. Lanthanides offer several advantages over other labels in that they are stable isotopes, there are a large number of them available, up to 100 or more distinct labels, they are relatively stable, and they are highly detectable and easily resolved between detection channels

when detected using mass spectrometry. Lanthanide labels also offer a wide dynamic range of detection. Lanthanides exhibit high sensitivity, are insensitive to light and time, and are therefore very flexible and robust and can be utilized in numerous different settings. Lanthanides are a series of fifteen metallic chemical elements with atomic numbers 57-71. They are also referred to as rare earth elements. Lanthanides may be detected using CyTOF technology. CyTOF is inductively coupled plasma time-of-flight mass spectrometry (ICP-MS). CyTOF instruments are capable of analysing up to 1000 cells per second for as many parameters as there are available stable isotope tags.

Typically, the binding partners are added to a suspension of cells, and incubated for a period of time sufficient to bind the available cell surface antigens. The incubation will usually be at least about 5 minutes and usually less than about 30 minutes. It is desirable to have a sufficient concentration of binding partners in the reaction mixture, such that the efficiency of the separation is not limited by lack of binding partners. The appropriate concentration is determined by titration. The medium in which the cells are separated will be any medium that maintains the viability of the cells.

In some embodiments, the level of CD160 in NK cells may also be quantified by single cell analysis. In some embodiments, the level of CD160 in NK cells may be quantified by single cell RNA sequencing. The method typically involves the steps of i) isolation of single cells; ii) lysis of the singles cells and extraction of the RNA molecules, iii) reverse transcription (RT) of said RNA molecules, iv) amplification of the cDNAs obtained at step C), v) cDNA pooling and purification, vi) preparation of a cDNA library, and, vii) sequencing said cDNA library. Typically the methods involves separation of individual cells into separate wells (e.g. by any cell sorting method such as FACS). More recent methods encapsulate individual cells in droplets in a microfluidic device, where the reverse transcription reaction takes place. Each droplet carries a DNA "barcode" that uniquely labels the cDNAs derived from a single cell. Once reverse transcription is complete, the cDNAs from many cells can be mixed together for sequencing; transcripts from a particular cell are identified by the unique barcode. Several scRNA-seq protocols have been published: Tang F, Barbacioru C, Wang Y, Nordman E, Lee C, Xu N, et al. (May 2009). "mRNA-Seq whole-transcriptome analysis of a single cell". Nature Methods. 6 (5): 377–82; Islam S, Kjällquist U, Moliner A, Zajac P, Fan JB, Lönnerberg P, Linnarsson S (July 2011). "Characterization of the single-cell transcriptional landscape by highly multiplex RNA-seq". Genome Research. 21 (7): 1160–7; Ramsköld D, Luo S, Wang

YC, Li R, Deng Q, Faridani OR, et al. (August 2012). "Full-length mRNA-Seq from single-cell levels of RNA and individual circulating tumor cells". Nature Biotechnology. 30 (8): 777–82; Hashimshony T, Wagner F, Sher N, Yanai I (September 2012). "CEL-Seq: single-cell RNA-Seq by multiplexed linear amplification". Cell Reports. 2 (3): 666–73; Singh M, Al-Eryani G, Carswell S, Ferguson JM, Blackburn J, Barton K, et al. (July 2019). "High-throughput targeted long-read single cell sequencing reveals the clonal and transcriptional landscape of lymphocytes". Nature Communications; Sasagawa Y, Nikaido I, Hayashi T, Danno H, Uno KD, Imai T, Ueda HR (April 2013). "Quartz-Seq: a highly reproducible and sensitive single-cell RNA sequencing method, reveals non-genetic gene-expression heterogeneity". Genome Biology. 14 (4): R31; Kouno T, Moody J, Kwon AT, Shibayama Y, Kato S, Huang Y, et al. (January 2019). "C1 CAGE detects transcription start sites and enhancer activity at single-cell resolution". Nature Communications. 10 (1): 360.

In some embodiments, the level of CD160 positively correlates with the patient's survival time. In some embodiments, the lower is the level of CD160, the higher is the probability that the patient will have a short survival time.

In some embodiments, the method of the present invention comprises the steps of i) determining the level of CD160 in the sample obtained from the patient, ii) comparing the level determined at step i) with a predetermined reference value and iii) concluding that the patient has a good prognosis when the level determined at step i) is higher than the predetermined reference value or concluding that the patient has a poor prognosis when the level determined at step i) is lower than the predetermined reference value.

As used herein, the term "**predetermined reference value**" refers to a threshold value or a cut-off value that discriminates the patients having a good prognosis from those having a poor prognosis. Typically, the predetermined reference value can be determined experimentally, empirically, or theoretically. A threshold value can also be arbitrarily selected based upon the existing experimental and/or clinical conditions, as would be recognized by a person of ordinary skilled in the art. For example, retrospective measurement of level of CD160 in properly banked historical subject samples may be used in establishing the predetermined reference value. The threshold value has to be determined in order to obtain the optimal sensitivity and specificity according to the function of the test and the benefit/risk balance (clinical consequences of false positive and false negative). Typically, the optimal sensitivity and specificity (and so the

threshold value) can be determined using a Receiver Operating Characteristic (ROC) curve based on experimental data. For example, after determining the level of CD160 in a group of reference, one can use algorithmic analysis for the statistic treatment of the measured expression levels of the gene(s) in samples to be tested, and thus obtain a classification standard having significance for sample classification. The full name of ROC curve is receiver operator characteristic curve, which is also known as receiver operation characteristic curve. It is mainly used for clinical biochemical diagnostic tests. ROC curve is a comprehensive indicator that reflects the continuous variables of true positive rate (sensitivity) and false positive rate (1-specificity). It reveals the relationship between sensitivity and specificity with the image composition method. A series of different cut-off values (thresholds or critical values, boundary values between normal and abnormal results of diagnostic test) are set as continuous variables to calculate a series of sensitivity and specificity values. Then sensitivity is used as the vertical coordinate and specificity is used as the horizontal coordinate to draw a curve. The higher the area under the curve (AUC), the higher the accuracy of diagnosis. On the ROC curve, the point closest to the far upper left of the coordinate diagram is a critical point having both high sensitivity and high specificity values. The AUC value of the ROC curve is between 1.0 and 0.5. When AUC>0.5, the diagnostic result gets better and better as AUC approaches 1. When AUC is between 0.5 and 0.7, the accuracy is low. When AUC is between 0.7 and 0.9, the accuracy is moderate. When AUC is higher than 0.9, the accuracy is quite high. This algorithmic method is preferably done with a computer. Existing software or systems in the art may be used for the drawing of the ROC curve, such as: MedCalc 9.2.0.1 medical statistical software, SPSS 9.0, ROCPOWER.SAS, DESIGNROC.FOR, MULTIREADER POWER.SAS, CREATE-ROC.SAS, GB STAT VI0.0 (Dynamic Microsystems, Inc. Silver Spring, Md., USA), etc.

In some embodiments, the predetermined reference value is determined by carrying out a method comprising the steps of a) providing a collection of samples; b) providing, for each ample provided at step a), information relating to the actual clinical outcome for the corresponding subject (i.e. the duration of the survival); c) providing a serial of arbitrary quantification values; d) determining the level of CD160 for each sample contained in the collection provided at step a); e) classifying said samples in two groups for one specific arbitrary quantification value provided at step c), respectively: (i) a first group comprising samples that exhibit a quantification value for level that is lower than the said arbitrary quantification value contained in the said serial of quantification values; (ii) a second group

comprising samples that exhibit a quantification value for said level that is higher than the said arbitrary quantification value contained in the said serial of quantification values; whereby two groups of samples are obtained for the said specific quantification value, wherein the samples of each group are separately enumerated; f) calculating the statistical significance between (i) the quantification value obtained at step e) and (ii) the actual clinical outcome of the subjects from which samples contained in the first and second groups defined at step f) derive; g) reiterating steps f) and g) until every arbitrary quantification value provided at step d) is tested; h) setting the said predetermined reference value as consisting of the arbitrary quantification value for which the highest statistical significance (most significant) has been calculated at step g).

For example the level of CD160 has been assessed for 100 samples of 100 subjects. The 100 samples are ranked according to the level of CD160. Sample 1 has the highest level and sample 100 has the lowest level. A first grouping provides two subsets: on one side sample Nr 1 and on the other side the 99 other samples. The next grouping provides on one side samples 1 and 2 and on the other side the 98 remaining samples etc., until the last grouping: on one side samples 1 to 99 and on the other side sample Nr 100. According to the information relating to the actual clinical outcome for the corresponding subject, Kaplan Meier curves are prepared for each of the 99 groups of two subsets. Also for each of the 99 groups, the p value between both subsets was calculated. The predetermined reference value is then selected such as the discrimination based on the criterion of the minimum p value is the strongest. In other terms, the level of CD160 corresponding to the boundary between both subsets for which the p value is minimum is considered as the predetermined reference value.

It should be noted that the predetermined reference value is not necessarily the median value of level of CD160. Thus in some embodiments, the predetermined reference value thus allows discrimination between a poor and a good prognosis for a patient. Practically, high statistical significance values (e.g. low P values) are generally obtained for a range of successive arbitrary quantification values, and not only for a single arbitrary quantification value. Thus, in one alternative embodiment of the invention, instead of using a definite predetermined reference value, a range of values is provided. Therefore, a minimal statistical significance value (minimal threshold of significance, e.g. maximal threshold P value) is arbitrarily set and a range of a plurality of arbitrary quantification values for which the statistical significance value calculated at step g) is higher (more significant, e.g. lower P value) are retained, so that a range of

quantification values is provided. This range of quantification values includes a "cut-off" value as described above. For example, according to this specific embodiment of a "cut-off" value, the outcome can be determined by comparing the level of CD160 with the range of values which are identified. In some embodiments, a cut-off value thus consists of a range of quantification values, e.g. centered on the quantification value for which the highest statistical significance value is found (e.g. generally the minimum p value which is found). For example, on a hypothetical scale of 1 to 10, if the ideal cut-off value (the value with the highest statistical significance) is 5, a suitable (exemplary) range may be from 4-6. For example, a subject may be assessed by comparing values obtained by measuring the level of CD160, where values higher than 5 reveal a poor prognosis and values less than 5 reveal a good prognosis. In some embodiments, a subject may be assessed by comparing values obtained by measuring the level of CD160 and comparing the values on a scale, where values above the range of 4-6 indicate a poor prognosis and values below the range of 4-6 indicate a good prognosis, with values falling within the range of 4-6 indicating an intermediate occurrence (or prognosis).

The invention will be further illustrated by the following figures and examples. However, these examples and figures should not be interpreted in any way as limiting the scope of the present invention.

FIGURES:

Figure 1. Frequencies of CD160-expressing cells among total NK cells from 5 healthy donors and 7 donors with AML. Statistical significance was assessed by Friedmann analysis with Dunn post-hoc tests on paired subset measurements, and *p*-values were adjusted with the Benjamini-Hochberg method. Error bars indicate the mean (± SD). * *p*-value<0.05, ** *p*-value<0.01, *** *p*-value<0.001, **** *p*-value<0.0001.

Figure 2. Kaplan-Meier curves for overall survival stratified by CD160 expression level in AML patients from TCGA. The optimal cut-off for patient stratification was obtained with a Cox proportional hazards model and the p-value was calculated in a log-rank test. CD160-high group (>= 7.427, n=78); CD160-low group (< 7.427, n=83).

EXAMPLE:

Samples

Frozen healthy bone marrow samples were recovered from filters used for allogeneic hematopoietic graft preparation. The use of such cells for scientific research is approved by the

French authorities in accordance with the regulations in force (authorization DC 2018-3143). Frozen bone marrow samples obtained from patients with AML at diagnosis were selected from an anonymized database registered with the "Commission Nationale de l'Informatique et des Libertés" (the French data protection agency; authorization no. FbP1089790#), and provided by the "Centre de Ressources Biologiques Cancer, Bordeaux Biothèques Santé" at Bordeaux University Hospital. Written informed consent was obtained from each patient for the use of biological samples for research, in accordance with the Declaration of Helsinki. Detailed information about the donors is provided in Supplementary Tables 1 and 2. This study was performed in accordance with French law (Art. L.1243-1 and Art. L.1245-2 of the French Public Health Code).

Cell preparation and NK cell enrichment

Samples were maintained in liquid nitrogen, sent with dry ice and stored either in liquid nitrogen or at -80°C if processing was planned shortly after arrival. On the day of processing, samples were thawed and put in a RPMI + 20% FCS medium containing DNase I (Roche). Cells were then washed with DPBS + 5% FCS + 2 mM EDTA. Cell viability was assessed with Trypan Blue dye. Cells were then transferred into a 5mL FACS tube, washed with FACS buffer. NK cells were then enriched by magnetic labelling of the contaminating cells with Miltenyi's NK cell isolation kit resulting in the specific enrichment of untouched NK cells.

NK cell sorting by flow cytometry

After enrichment, cells were washed and incubated at 1/50 with mouse serum (Sigma-Aldrich) for 10 min at 4°C. Cells were stained with anti-CD3 (clone UCHT1, FITC, Beckman Coulter), -CD14 (clone RMO52, FITC, Beckman Coulter), -CD19 (clone J3-119, FITC, Beckman Coulter) -CD45 (clone HI30, APC-Cy7, Biolegend) and -CD56 (clone N901(NKH-1), PE, Beckman Coulter) for 30 min at 4°C. We added an anti-CD34 (clone 581, FITC, BD Biosciences) to the lineage to sort AML samples. Cells were then washed twice with DPBS and incubated in DPBS with dead cell marker for 10 min at 4°C. Cells were washed again and sorted on an Influx or Melody cell sorter from BD (Becton Dickinson, San Diego, USA).

Single-cell RNA sequencing

After sorting, cells were washed in DPBS + 0.04% BSA, as recommended by the sample preparation protocol of 10x Genomics, and kept on ice until counting. We used the 10x Genomics Chromium single-cell 3' v2 kit and protocol to prepare the libraries. HalioDx

(Marseille, France) performed the RNA sequencing on a NextSeq500 machine with a sequencing depth of at least 50,000 reads per cell.

Flow cytometry to assess cell-surface phenotype

Frozen bone marrow from healthy and AML patients were thawed with DNAse I (Roche) and stained the following day, with antibodies against CD122 (clone Mik-β3, BV786, BD Biosciences), CD127 (clone HIL-7R-M21, Pe-Cy7, BD Biosciences), CD14 (clone M5E2, BUV737, BD Biosciences), CD16 (clone 3G8, BUV737, BD Biosciences), CD160 (clone BY55, Alexa Fluor® 488, BD Biosciences), CD19 (clone SJ25C1, BUV737, BD Biosciences), CD27 (clone M-T271, PerCP-Cy™5.5, BD Biosciences), CD3 (clone UCHT1, BUV496, BD Biosciences), CD45 (clone 2D1, APC-H7, BD Biosciences), CD52 (clone 4C8, Alexa Fluor® 647, BD Biosciences), CD56 (clone B159, Pe-Cy7, BD Biosciences), CD69 (clone FN50, BV605, BD Biosciences), perforin (clone δG9, PE-CF594, BD Biosciences), KIR2DL2/L3/S2 (clone GL183, PE-Cy5, Beckman Coulter), CD45 (clone HI30, APC-Cy7, Biolegend), Dead cell marker (BV510, Invitrogen), KIR2DL1/S1 (clone 11PB6, PE-Vio770, Miltenyi). Samples were run on a LSR II cytometer with UV-configuration from BD (Becton Dickinson, San Diego, USA). NK cells were defined as $CD3^-$ $CD56^+$ or $CD3^-$ $CD14^-$ $CD19^-$ $CD56^+$ cells. Statistical significances were calculated using Friedmann analysis with Dunn post hoc tests on paired subsets measurements, or a Dunn test and *p*-values were adjusted with the Benjamini-Hochberg method.

* *p*-value < 0.05, ** *p*-value < 0.01, *** *p*-value < 0.001, **** *p*-value < 0.0001.

Preprocessing of samples

Raw FASTQ files were processed with CellRanger software (v3.0.0 or 3.0.1), which performs alignment, filtering, barcode counting and UMI counting. CellRanger software was used to align reads with the GRch38 genome. Low-quality cells were excluded in an initial quality-control (QC) step, which removed genes expressed in fewer than three cells, and cells expressing fewer than 200 genes. Cells with less than 10% ribosomal genes for healthy controls and less than 15% ribosomal genes for AML samples were excluded. We also excluded cells more than 3 median absolute deviations (MADs) from the median value for UMI counts. In total, 23,850 healthy and 15,046 AML cells were retained for further analysis. Library-size normalization was performed on the UMI-collapsed gene expression values for each cell

barcode, with scaling by the total number of transcripts and multiplication by 10,000. The data were then log-transformed before further downstream analysis with Seurat (Satija et al., 2015).

Sample analysis

We first considered each donor separately. We selected genes with a high variance, using the FindVariableGenes function with default parameters. We then reduced the dimensionality of our data by principal component analysis (PCA) and selected the number of variable PCs retained by random sampling. Cells were clustered with Seurat's FindClusters function, with the Louvain algorithm. We tested a range of cluster resolution parameters and selected the parameter validated by the machine learning approach of Valentine Svensson used in one of our previous studies (http://www.nxn.se/valent/2018/3/5/actionable-scrna-seq-clusters) (Crinier et al., 2018). We removed cells assigned to clusters accounting for less than 2% of the cells, to avoid doublets, and we also removed a small cluster of cells from two donors that clustered away from the others and probably resulted from ILC contamination (87 and 32 cells, respectively). These cells had a high ILC score (as shown below). We also removed a donor-specific subset of 37 cells not found in seven other donors. We checked for the absence of any remaining contamination with the SingleR package (Aran et al., 2019). For visualization, we applied RunTsne and RunUmap to the cell loadings of the previously selected PCs with default parameters, to view the cells in two dimensions. We identified cluster markers with FindAllMarkers, with the parameter only.pos set to TRUE, to obtain only upregulated genes as markers of a cluster relative to all other cells. Marker genes were defined as genes with an adjusted p-value < 0.05 in a non-parametric Wilcoxon rank-sum test.

Pooled sample analysis

We pooled samples with the CellRanger aggregate function and subjected them to normalization, to equalize read depth between libraries. We performed regression on the runs, to overcome a batch effect that divided human healthy bone marrow NK cell samples into two categories on the basis of processing. We created three different pools of samples: a pool of healthy donor bone marrow NK cells, a pool of bone marrow NK cells from donors with AML and a pool of both these other pools. We then analyzed the pooled samples as described above.

Assessment of NK cell purity

We checked for ILC contamination in these pools by scoring our cells with the AddModuleScore function (Seurat) and the gene signatures of Björklund et al., (Bjorklund et

al., 2016) for ILCs and Hanna et al., (Hanna et al., 2004) for NK cells. The ILC signature was obtained from Björklund et al., (Bjorklund et al., 2016), by selecting the genes from NKvsILC1,2,3 that were upregulated in ILCs and for which the *p*-value was less than 0.05. The NK cell gene signature was obtained from Hanna et al., (Hanna et al., 2004) by merging the $CD56^{bright}CD16^{-}$vs$CD56^{dim}CD16^{+}$ upregulated gene list with the $CD56^{bright}CD16^{-}$ vs$CD56^{dim}CD16^{+}$ downregulated genes, both sorted with FC>2. This resulted in the additional removal of 10 cells from the bone marrow of healthy donors and 41 from the bone marrow of AML donors.

Unsupervised hierarchical clustering

We calculated the mean expression level of genes with variable expression across clusters and performed hierarchical clustering with these values. For all samples, a Euclidean distance was used for samples, genes and clusters.

Principal component analysis

PC component clustering analysis was performed with the Ade4 package, on the mean expression level of all genes, between clusters. PCA gene loadings for PC1 and PC2 corresponded to the genes making the largest contributions, accounting for 20% of the total information for each PC.

Heatmap

Heatmaps were generated from the scaled expression (log-normalized UMI counts) values for the discriminating gene sets defining each subset, with an adjusted *p*-value < 0.05 for a nonparametric Wilcoxon rank-sum test. The color scale is based on the *z*-score distribution.

Gene annotations

Cell membrane, secreted and transcription factor annotations were retrieved from public databases (Uniprot, MGI, and NCBI for mice and Uniprot, Genecards, and The Human Protein Atlas for humans). Genes encoding transcription factors were defined as such only if "transcription factor activity" was found among the GO annotations for the gene, to prevent the confusion of cofactors and coregulators with transcription factors.

GO enrichment analysis

We performed GO enrichment analysis with BiomaRt (Durinck et al., 2009) and the GOstats package (Falcon and Gentleman, 2007). Enrichment scores (*p*-values) for selected GO annotations were calculated with a hypergeometric statistical test with a significance threshold of 0.05. The data were plotted as -log10 of the *p*-value after Benjamini and Hochberg correction. The significance threshold was set at -log10(0.05).

Comparison with known NK cell subsets

Module scores for $CD56^{bright}$ and $CD56^{dim}$, hNK1 and hNK2, hNK_Sp1, hNK_SP2, hSP3 gene expression programs, as defined by Hanna et al. (Hanna et al., 2004) and Crinier et al., (Crinier et al., 2018), were determined with AddModuleScore from Seurat for each of our NK cells, at the single-cell level. Briefly, the mean expression level for each gene in the defined expression programs was calculated for each cell and the aggregated expression for control gene sets was then subtracted. All analyzed genes were binned on the basis of mean expression, and the control genes were randomly selected from each bin. A violin plot representation was used to assess the distribution of module scores for each NK cell, grouped by subset. Statistical significance was calculated in a Wilcoxon rank sum test with continuity correction or in a Kruskal-Wallis test plus Dunn's multiple-comparison test, with *p*-value adjustment by the Benjamini-Hochberg method: * p-value < 0.05, ** p-value < 0.01, *** p-value < 0.001, **** p-value < 0.0001.

Pseudotime

For the bone marrow, we performed pseudotime analysis with Monocle3 (v0.1.3) and the cells filtered with Seurat, as described above, for each sample individually. We imported Seurat clustering and NK/NKP scoring metadata into the analysis. The starting point of the trajectory was defined as the end point of the branch with the highest NKP signature score.

For the spleen, we used our previously published dataset (Crinier et al., 2018), and pseudotime analysis was again performed with Monocle 3 (v0.1.3). The starting point of the trajectory was defined as the end point of the branch with the lowest mature NK cell score, and cluster assignments were retrieved from our previous analysis.

Definition of the NK cell vs. NKP gene signature

Affymetrix CEL files were analyzed with the limma package (v3.34.9), with RMA normalization. Genes with an adjusted p value<0.01 were considered to be differentially expressed.

Definition of the canonical vs. adaptive NK cell gene signature

RNA-seq analysis was performed with the DESeq2 package (v1.26.0). Genes with a log2 fold change in expression >1 and an adjusted *p* value<0.05 were considered to be differentially expressed.

Results:

High-throughput scRNA-Seq identifies adaptive NK cells in the human bone marrow

We investigated the heterogeneity of human bone marrow NK cells with the 10xGenomics high-throughput droplet-based scRNA-Seq pipeline, which can be used for the unbiased transcriptomic characterization of thousands of cells simultaneously (Zheng et al., 2017). We analyzed ~24,000 flow cytometry-sorted NK cells, defined as $CD3^-CD14^-CD19^-CD56^+$ cells, from the bone marrow of eight healthy donors. We checked that Lin^-CD56^+ helper-like ILCs were absent from this population, using a module score analysis comparing single-cell human NK cell and helper-like ILC gene signatures, as previously described (Bjorklund et al., 2016; Hanna et al., 2004). This resulted in the removal of only 10 contaminating helper-like ILCs from the ~24,000 cells analyzed (**data not shown**). We analyzed bone marrow NK cell heterogeneity, by projecting cells onto two dimensions in a uniform manifold approximation and projection (UMAP) analysis. UMAP analysis revealed the clustering of human bone marrow NK cells into four different subsets, referred to hereafter as hNK_Bm1, hNK_Bm2, hNK_Bm3, and hNK_Bm4 cells (**data not shown**). The three main NK cell subsets (hNK_Bm1, hNK_Bm2, hNK_Bm3) were common to all samples, whereas the hNK_Bm4 subset was absent from some donors (**data not shown**).

We first focused on hNK_Bm4 and identified 139 differentially expressed genes distinguishing this cluster from the other human bone marrow NK cell subsets: 88 of these genes were downregulated in hNK_Bm4 and 51 were upregulated (**data not shown**). We found that hNK_Bm4 cells had lower levels of expression for the *KLRB1* and *CD7* genes encoding activating receptors, *KLRC1* (encoding NKG2A) and *SIGLEC7*, encoding inhibitory receptors, *IL2RB*, encoding the IL-2/IL-15Rβ (CD122) surface receptor essential for the development and differentiation of NK cells (Huntington et al., 2009), and *FCER1G* (FcRγ) (**data not shown**). By contrast, hNK_Bm4 cells had higher levels of expression for genes encoding NK cell-associated effector proteins (*CCL5*, *GZMM*, and *GZMH)* (Cooper et al., 2001; Hanna et al., 2004) and *ZEB2,* encoding a transcriptional regulator involved in terminal NK cell maturation

(van Helden et al., 2015). Gene ontology (GO) term analysis revealed that hNK_Bm4 cells were specifically enriched in NK cell effector functions, such as the positive regulation of interferon (IFN)-γ production, NK cell-mediated cytotoxicity and granzyme-mediated apoptotic signaling (**data not shown**). The hNK_Bm4 subset also displayed an upregulation of several genes relating to the class II major histocompatibility complex (MHC), T cell co-stimulation, and the regulation of T-cell activation and proliferation (**data not shown**). The hNK_Bm4 subset was identified in three of the five donors seropositive for human cytomegalovirus (HCMV) (Table S1). *FCER1G* downregulation (**data not shown**) and GO term enrichment for antigen presentation and T-cell activation (**data not shown**) are properties also displayed by adaptive NK cells (Costa-Garcia et al., 2019; Liu et al., 2016; Liu et al., 2015; Schlums et al., 2015). We therefore investigated whether the hNK_Bm4 subset could be considered to correspond to adaptive NK cells. We established canonical and adaptive NK cell gene signatures, by analyzing the transcriptomic profiles of human blood $CD3^-CD56^{dim}CD57^+NKG2C^+$ adaptive and $CD3^-CD56^{dim}CD57^-NKG2C^-$ canonical NK cells from a public genome-wide RNAseq dataset (Cichocki et al., 2018) (**data not shown**). Unsupervised hierarchical clustering (**data not shown**) and principal component analysis (PCA) (**data not shown**) segregated the samples into two groups, corresponding to adaptive and canonical NK cells. A bilateral comparison of the two populations identified 912 from the total gene set as being differentially expressed (**data not shown**). These genes included *KLRC2* (encoding NKG2C) (**data not shown**), which was overexpressed in adaptive NK cells. The expression of this gene is associated with the adaptive phenotype of NK cells during cytomegalovirus infection (Beziat et al., 2013). The top 200 genes of both these gene signatures intersected broadly with the genes detected in our scRNAseq dataset, which included 173 of the top 200 driver genes of the adaptive gene signature and 174 of the top 200 driver genes of the canonical gene signature (**data not shown**), indicating comparability. Module score analysis comparing the adaptive and canonical gene signatures of each of the bone marrow NK cell subsets revealed that the gene expression profile of hNK_Bm4 cells most closely resembled that of adaptive NK cells (**data not shown**). Violin plots of module scores between subsets also revealed a significant enrichment in the gene signature of adaptive NK cells for hNK_Bm4 (**data not shown**). The hNK_Bm4 subset therefore had a transcriptomic profile different from that of conventional NK, closely resembling that of adaptive NK cells, suggesting that adaptive NK cells may populate the bone marrow of some HCMV-seropositive individuals.

Three NK cell subsets are present in human bone marrow at steady state

For further characterization of the heterogeneity of bone marrow NK cells among donors, we removed the hNK_Bm4 adaptive NK cell-like NK cell subset, which was absent from some donors, from the analysis. Unsupervised hierarchical clustering (data not shown) and UMAP analysis on the remaining ~23,000 human bone marrow NK cells again clustered the cells into three different subsets: hNK_Bm1, hNK_Bm2 and hNK_Bm3 (**data not shown**). These three subsets were present in all samples (**data not shown**). Significant differential expression between the hNK_Bm1, hNK_Bm2 and hNK_Bm3 subsets was observed for 261 of the total genes composing the three different transcriptomic signatures of bone marrow NK cells (**data not shown**). No significant individual-specific phenotype or batch effect was observed and in the unsupervised hierarchical clustering (data not shown), and the NK subsets from a given individual did not cluster together on the PC analysis (**data not shown**). Instead, PC1 and PC2, accounting for 42% and 22% of the variance, respectively, and unsupervised hierarchical clustering (data not shown) segregated the eight donors into three different groups corresponding to hNK_Bm1, hNK_Bm2 and hNK_Bm3 (**data not shown**). PC1 separated the hNK_Bm1, hNK_Bm2 and hNK_Bm3 subsets. The hNK_Bm3 subset was also separated from hNK_Bm1 and hNK_Bm2 by PC2. The *GNLY* and *GZMB* genes associated with cell cytotoxicity were identified as drivers for hNK_Bm1 on PC1. *CD160,* encoding an NK cell activating receptor, and *CCL3* and *CCL4,* encoding chemokines, were identified as drivers of the hNK_Bm2 subset, whereas *ZFP36L2* (which is involved in lymphocyte hematopoiesis (Stumpo et al., 2009; Zhang et al., 2013)) and *DUSP2* (a regulator of the ERK pathway) were drivers of the hNK_Bm3 subset on PC1 and PC2 (**data not shown**).

We then analyzed the top ten genes encoding secreted proteins, cell membrane markers and transcription factors expressed in hNK_Bm1, hNK_Bm2, and hNK_Bm3 cells (**data not shown**). hNK_Bm1 cells displayed an upregulation of genes associated with cytotoxic factors (*FGFBP2*, *GZMB*, *GZMH*, and *PRF1*), and overexpressed *FCGR3A* (encoding CD16), which is characteristic of the $CD56^{dim}$ NK cell subset (Liu et al., 2016; Liu et al., 2015; Schlums et al., 2015), and *S1PR5,* which encodes a sphingosine 1-phosphate receptor promoting NK cell egress from lymph nodes and bone marrow (Walzer et al., 2007a) (**data not shown**). The hNK_Bm2 subset displayed enrichment for genes encoding soluble factors associated with NK cell effector functions (*CCL3*, *CCL4*, *XCL1*, *XCL2*, *GZMK* and *CCL3L1*), amphiregulin (*AREG*), the activating receptor encoded by *CD160*, the activation marker encoded by *CD69*, and the chemokine receptor encoded by *CXCR6,* which is involved in ILC egress from the bone

marrow (Chea et al., 2015) (**data not shown**). Like hNK_Bm2 cells, the hNK_Bm3 subset displayed higher levels of expression for *GZMK*, *XCL1*, *XCL2* and *AREG*, but these cells also displayed an upregulation of the *LTB*, *SELL* (encoding CD62L) and *CD44* genes encoding adhesion molecules associated with homing and anchorage in the bone marrow (Avigdor et al., 2004; Burgess et al., 2013) (**data not shown**). Biological process enrichment analysis revealed a specific enrichment of the hNK_Bm1 subset in the FcγR signaling pathway, the granzyme-mediated apoptotic signaling pathway and cytolysis (**data not shown**). By contrast, the hNK_Bm2 and hNK_Bm3 subsets both displayed enrichment in chemokine and cytokine responses, cytokine production and cytokine-mediated signaling. The hNK_Bm2 subset was more strongly enriched in responses and the hNK_Bm3 subset was more specifically enriched in IL-2 production. These results thus reveal the presence of three different subsets of human bone marrow NK cells at steady state.

The three human bone marrow NK cell subsets encompass an NK1-CD56^{dim}-like subset, a NK2-CD56^{bright}-like subset and an additional CD56^{bright}-like subset

We then compared the transcriptomic signatures of the three human bone marrow NK cell subsets with those of the blood and splenic NK1 and NK2 subsets, which resembled CD56^{dim} and CD56^{bright} cells, respectively, and two additional spleen-specific hNK_Sp3 and hNK_Sp4 human NK cell populations, as previously described (Crinier et al., 2018; Hanna et al., 2004). Gene signature heatmaps (**data not shown**) and module score analysis (**data not shown**) revealed that hNK_Bm1 cells corresponded to NK1, the related splenic hNK_Sp1 and CD56^{dim} NK cells, consistent with the pattern of *FCGR3A* expression. hNK_Bm2 corresponded to NK2, the related hNK_Sp2 and CD56^{bright} NK cells (**data not shown**). Further analysis revealed that the hNK_Bm3 subset shared part of the NK2 gene signature but was most like the minor hNK_Sp3 subset residing in the spleen (**data not shown**). No hNK_Sp4 subset signature was found in bone marrow NK cells (**data not shown**).

A flow cytometry analysis of bone marrow NK cells revealed that the expression of CD160 and CD52 (CAMPATH-1) at the cell surface of CD56^{bright} cells was mutually exclusive, further discriminating between hNK_Bm2 and 3, respectively, as previously reported for hNK_Sp2 and 3 in the spleen (Crinier et al., 2018) (**data not shown**). These analyses showed that the human bone marrow NK cell compartment consists mostly of CD56^{dim} NK cells (~50%), with a few CD56^{bright}-like CD160^{+}CD52^{-} NK cells (~10%) and CD56^{bright} CD160^{-}CD52^{+} NK cells (~5%) (**data not shown**). Protein levels for perforin, KIR2DL2/2DL3 and KIR2DL1/2DS1

were higher in $CD56^{dim}$-like cells than in $CD56^{bright}$-like $CD160^{+}CD52^{-}$ NK cells and $CD56^{bright}$ $CD160^{-}CD52^{+}$ NK cells, confirming our transcriptomic data (**data not shown**). The hNK_Bm2 subset was characterized by higher levels of CD122, CD27 and CD69, whereas hNK_Bm3 cells had higher levels of CD127 (**data not shown**).

Together, these results demonstrate that hNK_Bm1 and hNK_Bm2 subsets resemble the NK1-$CD56^{dim}$ and NK2-$CD56^{bright}$ subsets respectively, which also populate the human blood and spleen. The third subset, hNK_Bm3, most closely resembled the hNK_Sp3 population resident in the spleen and absent from the bloodstream.

The NK0 subset has features consistent with a role as the precursor to both the NK2 and NK1 subsets

We then investigated whether the three NK cell subsets identified in the bone marrow reflected differences in maturation status. *KLRC1* (encoding NKG2A) was expressed at higher levels in the hNK_Bm2 and hNK_Bm3 subsets, whereas expression of the killer-cell immunoglobulin-like receptors (KIRs) KIR2DL3 and KIR3DL1 was restricted to the hNK_Bm1 subset (**data not shown**). These results suggest that the hNK_Bm1 subset is more mature than the hNK_Bm2 and hNK_Bm3 subsets, because a decrease in the cell surface expression of NKG2A and a concomitant increase in KIR expression has been associated with human NK cell differentiation (Beziat et al., 2010). We then searched for a developmental path across bone marrow NK subsets, by applying the pseudotime algorithm Monocle DDR Tree, which computationally orders the transcriptomic profiles of cells along a trajectory, without prior information about their clustering (Trapnell et al., 2014). The pseudotime algorithm ordered cells along a trajectory segregating our ~23,000 bone marrow NK cells into two branches and three clusters. hNK_Bm3 subset is at the intersection of two branches linking hNK_Bm1-hNK_Bm3 subsets, and hNK_Bm2-hNK_Bm3 subsets. These three clusters overlapped perfectly with the hNK_Bm1, hNK_Bm2 and hNK_Bm3 subsets defined by the UMAP analysis, providing additional support for our previous conclusions (**data not shown**).

We then tried to define the starting point of the putative developmental trajectory, by comparing our dataset with an NK cell precursor (NKP) gene signature. We examined the transcriptomic profiles of bone marrow $Lin^{-}CD34^{+}CD38^{+}CD123^{-}CD45RA^{+}CD7^{+}CD10^{+}CD127^{-}$ NKP and $CD3^{-}CD56^{+}NKp46^{+}$ mature NK cells from a public genome-wide RNAseq dataset (Renoux et al., 2015). Unsupervised hierarchical clustering separated the samples into two main branches

on the basis of precursor or mature NK cell phenotype, suggesting that these two populations could be differentiated on the basis of a specific transcriptomic pattern (**data not shown**). PCA confirmed this finding, as mature NK cells clustered away from progenitors along a combined PC1 and PC2 axis, accounting for 30.7% and 16.6% of the total variance, respectively (**data not shown**). A bilateral comparison of the two populations identified 448 genes from the total gene set as differentially expressed, with 265 upregulated in NK cells and 183 genes upregulated in progenitors (**data not shown**). Mature NK cells had higher levels of *CD160*, *FCGR3A*, *GZMB* and *CCL3* expression, whereas NK cell progenitors displayed an upregulation of *TCF4* and *RAG2,* which are expressed during NK cell development (Leavy, 2014) (**data not shown**). These gene signatures broadly intersected with the genes detected by our scRNAseq results, with 263 genes from the mature NK cell signature and 160 genes from the progenitor gene signature found in our dataset (**data not shown**). Module score analyses comparing NKP and mature NK cell gene signatures between bone marrow NK cell subsets were applied to the developmental trajectory defined by the pseudotime algorithm (**data not shown**). This analysis revealed that the hNK_Bm3 subset displayed specific enrichment in the NKP signature, whereas the hNK_Bm1 subset was enriched in the mature NK cell profile (**data not shown**). Violin plots of NKP gene signature module score also showed the hNK_Bm3 subset to be the most immature, followed by hNK_Bm2, with the hNK_Bm1 subset the most mature (**data not shown**). The hNK_Bm3 subset was, therefore, defined as the starting point of the pseudotime developmental trajectory (**data not shown**).

Pseudotime analysis with Monocle DDR Tree revealed a specific developmental trajectory of human bone marrow NK cells, with the $CD56^{bright}$-like hNK_Bm3 minor subset differentiating into the NK1-$CD56^{dim}$-like hNK_Bm1 subset and a distinct NK2-$CD56^{bright}$-like hNK_Bm2 subset (**data not shown**). The NK1-$CD56^{dim}$-like hNK_Bm1 and NK2-$CD56^{bright}$-like hNK_Bm2 subsets followed distinct developmental pathways. Similar results were found using another pseudotime algorithm (PAGA Tree from Dynverse), further strengthening our putative differentiation trajectory (data not shown).

As for the bone marrow, we reanalyzed our previous splenic dataset (Crinier et al., 2018) with the recent pseudotime algorithm Monocle DDR Tree. Pseudotime analysis ordered splenic NK cells into two branches and four clusters that corresponded to the hNK_Sp1, hNK_Sp2, hNK_Sp3 and hNK_Sp4 subsets (**data not shown**). The hNK_Sp3 subset was identified as the least mature, followed by hNK_Sp2, and the hNK_Sp1 and hNK_Sp4 subsets were more

mature (**data not shown**). Thus, in the spleen, as in the bone marrow, a minor CD56^{bright}-like hNK_Sp3 subset differentiates into the NK1-CD56^{dim}-like hNK_Sp1 subset and a distinct NK2-CD56^{bright}-like hNK_Sp2 subset (**data not shown**). We therefore refer to the CD56^{bright}-like hNK_Bm3 and CD56^{bright}-like hNK_Sp3 subsets as NK0 hereafter (**data not shown**).

Acute myeloid leukemia affects the transcriptome of human bone marrow NK cells

Acute myeloid leukemia (AML), is a specific bone marrow disease and known to be associated with a strong impairment of NK cell function in the periphery (Chretien et al., 2017c). We therefore investigated the impact of AML on the heterogeneity of bone marrow NK cells. We analyzed ~15,000 flow cytometry-sorted bone marrow NK cells, defined as CD3$^-$CD14$^-$CD19$^-$CD34$^-$CD56$^+$ cells, from eight AML patients at diagnosis (**data not shown**). A module score analysis comparing human NK cell and helper-like ILC gene signatures resulted in the removal of 39 ILC-like cells (**data not shown**). UMAP analysis on the remaining cells revealed the existence of several NK cell subsets (**data not shown**), but their assignment on the basis of donor origin showed that these clusters had a strong donor phenotype (**data not shown**). There was no conserved NK cell subset in AML patients (data not shown). We then investigated whether module score analysis could be used to compare the specific signatures of each of the hNK_BM subsets to this AML dataset (**data not shown**). Module score analysis was applied to the UMAP representation of total NK cells from AML patients (**data not shown**). A high level of transcriptomic heterogeneity was observed at the patient scale, for both subset composition and percentages. Based on protein levels, we detected heterogeneity in the percentages of the CD56^{bright} and CD56^{dim} subsets between AML samples (**data not shown**). Thus, AML strongly affected the transcriptomic profile of bone marrow NK cells, making it impossible to analyze their heterogeneity with classical annotation tools.

We therefore investigated the effects of AML on bone marrow NK cells further, by analyzing a mixture of bone marrow NK cells from healthy donors and AML patients. UMAP analysis on the ~38,700 bone marrow NK cells revealed that NK cells clustered differentially according to the clinical status of the donor (**data not shown**). In total, 197 genes were differentially expressed between bone marrow NK cells from healthy donors and donors with AML: 90 genes were upregulated in NK cells from healthy donors, and 107 genes were upregulated in NK cells from donors with AML (**data not shown**). Bone marrow NK cells from AML patients had higher levels of expression for interferon-induced genes (*IFI44L*, *IFI6*, *IFIT3* and *IFI44*), HLA molecule-encoding genes (*HLA-DPB1*, *HLA-DPA1*, *HLA-DRB5*, *HLA-DRB1*) and *ZEB2* and

KLF2, encoding transcription factors controlling NK cell maturation (van Helden et al., 2015) and survival (Rabacal et al., 2016), respectively. By contrast, NK cells from the bone marrow of healthy donors displayed higher levels of expression for genes encoding NK cell effector molecules (CCL3, CCL4 and GZMM), genes encoding surface receptors (CD16 (*FCGR3A*), CD161 (*KLRB1*), NKG2A (*KLRC1*), CD300A, and FcγR (*FCER1G*), KIR2DL3, KIR2DL1 and CD160). The higher levels of CD160 expression in bone marrow NK cells from healthy donors than in bone marrow cells from donors with AML donors was confirmed by assessing protein levels by flow cytometry (**Figure 1**). Bone marrow NK cells from healthy donors also displayed stronger expression of genes involved in regulating NK cell effector functions (*DOCK2*, *EVL*, *LCK*, *RAP1B*, *LAT*, *JAK1*, *CORO1A* and *FGR* (Awasthi et al., 2010; Celis-Gutierrez et al., 2014; Huang et al., 2016; Jevremovic et al., 1999; Mace and Orange, 2014; Sasanuma et al., 2006; Wilton et al., 2019; Witalisz-Siepracka et al., 2018)), *PTPN6* (encoding SHIP-1) and *ITGB2,* which has been reported to promote NK cell response (Crozat et al., 2011; Viant et al., 2014).

Biological process enrichment analysis revealed an enrichment in the GO terms "response to cytokine" and "type I interferon signaling pathways" in bone marrow NK cells from AML patients (**data not shown**), relative to bone marrow NK cells isolated from healthy individuals. By contrast, NK cells purified from healthy bone marrow displayed an enrichment in the GO terms "NK cell-mediated cytotoxicity", "FcγR signaling pathway", "exocytosis", "response to IL-12" and "IL-15-mediated signaling pathways". Together, these results suggest that bone marrow NK cells from healthy donors have a more activated phenotype than those isolated from AML patients, which displayed a strong type I IFN response signature. We extended our analysis of NK cell transcriptomic profiles further, by assessing the enrichment in GO terms relating to cell metabolism (**data not shown**). Bone marrow NK cells from AML patients displayed an enrichment in GO terms associated with the regulation of gene expression through the processes of transcription, splicing, and epigenetic modifications, the regulation of macromolecules and metabolic processes and stress-related signaling, relative to bone marrow NK cells from healthy individuals. These results highlight the impact of AML disease on bone marrow NK cells.

We then investigated the potential role of CD160 in AML disease development and progression further, by studying the clinical outcome of cancer patients. Survival was much higher in

patients with CD160-high AML than in those with CD160-low cancer, suggesting that CD160 is an anti-tumor biomarker in AML (**Figure 2**).

Discussion:

The main objective of this study was to address, from an unbiased transcriptome-wide perspective, the heterogeneity of NK cells in human bone marrow at steady state and at the time of diagnosis of acute myeloid leukemia, a hematologic malignancy of the bone marrow.

We report here four different clusters of bone marrow Lin^-CD56^+ cells, hNK_Bm1, hNK_Bm2, hNK_Bm3 and hNK_Bm4, the last of which was not present in all donors. Unsupervised hierarchical clustering was further validated by machine learning supporting the robustness of our analysis. By contrast, scRNAseq profiling of human healthy bone marrow Lin^-CD7^+ cells yielded six NK cell clusters (Yang et al., 2019), with CD7 expressed by both progenitors and mature ILCs (Lim et al., 2017). Our analysis on Lin^-CD56^+ cells was thus expected to be different. Nevertheless, similarities can exist between the two studies as the 'mature' and 'terminal' populations characterized by *PRF1*, GZMB, *S100A6*, *FCGR3A*, *LGALS1*, and *SPON2* expression (Yang et al., 2019) resembled the hNK_Bm1 subset, the 'active' and 'transitional' populations expressing *CCL3, XCL2, PI3KR1, IRFD1* and *FOS* (Yang et al., 2019) resembled the hNK_Bm2 subset, and the $CD56^{bright}$ subset (Yang et al., 2019) resembled the $CD56^{bright}$ hNK_Bm3 subset, with the expression of *IL7R*, *CD44*, *LTB*, *XCL1*, *GZMK*, *SELL*, and *XCL2*.

We identified three subsets of NK cells in the bone marrow of all healthy humans, including the conserved NK1-$CD56^{dim}$-like and NK-$CD56^{bright}$-like subsets. Both the NK1 and NK2 subsets are, therefore, present in the blood, spleen and bone marrow. This finding is consistent with NK cells originating in the bone marrow and with their release into the bloodstream and continual recirculation throughout the body, leading to the population of several organs, including the spleen (Cooper et al., 2001; Yu et al., 2013). Consistent with our previous findings (Crinier et al., 2018), we observed that the NK1-$CD56^{dim}$ subset had a transcriptomic profile enriched in markers of cytotoxic activity, whereas the transcriptomic profile of NK2-$CD56^{bright}$ cells was more heavily enriched in genes involved in the response to cytokines and chemokines. We detected an additional NK0 $CD56^{bright}$-like subset, originally identified as hNK_Bm3, which resembled the hNK_Sp3 subset residing in the human spleen (Crinier et al., 2018). NK0 cells were not found in the blood, accounting for the previous lack of detection of this subset. The cells of this population expressed high levels of CD56 at their surface ($CD56^{bright}$), and could be distinguished from NK2 on the basis of their higher levels of CD52 and CD127

expression and lower levels of CD160 expression. We found that NK0 cells displayed specific enrichment in genes associated with the NK cell precursor (NKP) signature. The pseudotime algorithm Monocle DDR Tree, which infers developmental trajectories from scRNA-seq data, showed that bone marrow NK0 (hNK_Bm3) cells may differentiate into NK1 and NK2 cells (**data not shown**). Our data thus show that a minor subset of the $CD56^{bright}$ NK cell population, the tissue-resident $CD56^{bright}CD127^{+}CD160^{-}CD52^{+}$ cells, referred to hereafter as NK0 cells, can give rise to other NK2/$CD56^{bright}CD160^{+}CD52^{-}$ cells and to NK1/$CD56^{dim}$-perforin-^{high} cells. These results are consistent with previous studies showing that $CD56^{bright}$ NK cells can differentiate into $CD56^{dim}$ NK cells (Chan et al., 2007; Dulphy et al., 2008), and provide the first demonstration, at the transcriptomic level, of such differentiation in humans, *in vivo*. NK1 and NK2 cells appeared at the end of the two branches on the pseudotime representation, suggesting that these two populations were not developmentally related. This may explain why not all $CD56^{bright}$ cells differentiate into $CD56^{dim}$ cells (Chan et al., 2007).

Similar analyses for the human spleen showed that spleen NK0 (hNK_Sp3) cells may also differentiate into NK1 and NK2 cells. While it was supposed for a long time that NK cells develop exclusively within the bone marrow, it is now clear that some NK cell precursors are selectively enriched in extramedullar tissues (Freud et al., 2014). The biological relevance of extramedullar NK cell differentiation remains to be revealed, as well as the mechanisms that govern it.

In this study, we also used public datasets containing transcriptomic profiles of canonical and adaptive NK cells (Renoux et al., 2015) to obtain the first transcriptomic signature of human adaptive NK cells. Based on transcriptomic data, we detected adaptive NK cells in the bone marrow of human CMV-seropositive individuals. The presence of adaptive NK cells was correlated with CMV-seropositivity, but not all CMV-seropositive donors had adaptive NK cell subsets that were detectable, at least by transcriptomic analyses. These results are consistent with a previous study from Schlums and coworkers showing that not all CMV-seropositive individuals have circulating adaptive NK cells (Schlums et al., 2015).

A population of tissue-resident NK cells, named ltNK cells, has recently been described (Lugthart et al., 2016). These cells are absent from the blood but can account for ~29% of NK cells in the bone marrow, ~45% of splenic NK cells and ~56% of NK cells in lymph node (Lugthart et al., 2016). ltNK cells have a $CD69^{+}CXCR6^{+}$ cell surface phenotype but disparate levels of CD56 and CD16 (Lugthart et al., 2016), suggesting that this population is heterogeneous at least for the $CD56^{bright}$ and $CD56^{dim}$ subsets. The hNK_Bm3 and hNK_Sp3 subsets, corresponding to our NK0 tissue-resident progenitor, were not enriched in the

transcriptomic signature of ltNK defined by bulk RNAseq on flow cytometry cell-sorted $CD69^{+}CXCR6^{+}$ cells (Melsen et al., 2016). Given that RNAseq averages the gene expression profile of the population considered and that ltNK cells have a heterogenous surface phenotype, these cells may also have a heterogeneous transcriptomic profile, preventing their identification at the transcriptomic level by scRNAseq.

We tried to explore the heterogeneity of the bone marrow NK cell compartment in AML patients at diagnosis. We found that each sample had its own specific transcriptomic profile, preventing subset assignment. A similar patient-specific pattern was also recently observed for the expression of NKp30 and CD27 on the surface of NK cells from AML patients (Bruck et al., 2020). We were nevertheless able to extract a transcriptomic signature of NK cells in AML disease conditions relative to steady state. Bone marrow NK cells from AML patients had a transcriptomic profile enriched in responses to cytokine and type I interferon signaling pathways. Consistent with the well-known impairment of NK cell function during AML (Chretien et al., 2017c; Costello et al., 2002; Fauriat et al., 2007), NK cells isolated from healthy individuals had a transcriptomic profile enriched in genes involved in cell cytotoxicity, the FcγR receptor signaling pathway, exocytosis, the response to IL-12 and IL-15 -signaling pathways, indicating of a more activated NK cell phenotype for these cells than those isolated from AML patients. Impairment of NK cells from AML patient at the site of the disease onset was also consistent with the capacity of AML blast to affect NK cells *in vitro* (Khaznadar et al., 2014; Scoville et al., 2018; Stringaris et al., 2014).

Overall, our study reveals a NK0 $CD56^{bright}$-like subset as the precursor of NK1-$CD56^{dim}$ and NK2-$CD56^{bright}$ subsets. Our findings in AML pathology also showed that NK cells underwent a donor-specific cancer editing and documented further the profound NK cell impairment in the bone marrow at diagnosis.

REFERENCES:

Throughout this application, various references describe the state of the art to which this invention pertains. The disclosures of these references are hereby incorporated by reference into the present disclosure.

Abdul-Careem, M.F., Mian, M.F., Yue, G., Gillgrass, A., Chenoweth, M.J., Barra, N.G., Chew, M.V., Chan, T., Al-Garawi, A.A., Jordana, M., et al. (2012). Critical role of natural killer cells in lung immunopathology during influenza infection in mice. J Infect Dis 206, 167-177.

Aran, D., Looney, A.P., Liu, L., Wu, E., Fong, V., Hsu, A., Chak, S., Naikawadi, R.P., Wolters, P.J., Abate, A.R., et al. (2019). Reference-based analysis of lung single-cell sequencing reveals a transitional profibrotic macrophage. Nat Immunol 20, 163-172.

Avigdor, A., Goichberg, P., Shivtiel, S., Dar, A., Peled, A., Samira, S., Kollet, O., Hershkoviz, R., Alon, R., Hardan, I., et al. (2004). CD44 and hyaluronic acid cooperate with SDF-1 in the trafficking of human CD34+ stem/progenitor cells to bone marrow. Blood 103, 2981-2989.

Awasthi, A., Samarakoon, A., Chu, H., Kamalakannan, R., Quilliam, L.A., Chrzanowska-Wodnicka, M., White, G.C., 2nd, and Malarkannan, S. (2010). Rap1b facilitates NK cell functions via IQGAP1-mediated signalosomes. J Exp Med 207, 1923-1938.

Beziat, V., Descours, B., Parizot, C., Debre, P., and Vieillard, V. (2010). NK cell terminal differentiation: correlated stepwise decrease of NKG2A and acquisition of KIRs. PLoS One 5, e11966.

Beziat, V., Liu, L.L., Malmberg, J.A., Ivarsson, M.A., Sohlberg, E., Bjorklund, A.T., Retiere, C., Sverremark-Ekstrom, E., Traherne, J., Ljungman, P., et al. (2013). NK cell responses to cytomegalovirus infection lead to stable imprints in the human KIR repertoire and involve activating KIRs. Blood 121, 2678-2688.

Bjorklund, A.K., Forkel, M., Picelli, S., Konya, V., Theorell, J., Friberg, D., Sandberg, R., and Mjosberg, J. (2016). The heterogeneity of human CD127(+) innate lymphoid cells revealed by single-cell RNA sequencing. Nat Immunol 17, 451-460.

Bjorkstrom, N.K., Lindgren, T., Stoltz, M., Fauriat, C., Braun, M., Evander, M., Michaelsson, J., Malmberg, K.J., Klingstrom, J., Ahlm, C., et al. (2011). Rapid expansion and long-term persistence of elevated NK cell numbers in humans infected with hantavirus. J Exp Med 208, 13-21.

Bjorkstrom, N.K., Ljunggren, H.G., and Michaelsson, J. (2016). Emerging insights into natural killer cells in human peripheral tissues. Nat Rev Immunol 16, 310-320.

Bruck, O., Dufva, O., Hohtari, H., Blom, S., Turkki, R., Ilander, M., Kovanen, P., Pallaud, C., Ramos, P.M., Lahteenmaki, H., et al. (2020). Immune profiles in acute myeloid leukemia bone marrow associate with patient age, T-cell receptor clonality, and survival. Blood Adv 4, 274-286.

Burgess, M., Gill, D., Singhania, R., Cheung, C., Chambers, L., Renyolds, B.A., Smith, L., Mollee, P., Saunders, N., and McMillan, N.A. (2013). CD62L as a therapeutic target in chronic lymphocytic leukemia. Clin Cancer Res 19, 5675-5685.

Celis-Gutierrez, J., Boyron, M., Walzer, T., Pandolfi, P.P., Jonjic, S., Olive, D., Dalod, M., Vivier, E., and Nunes, J.A. (2014). Dok1 and Dok2 proteins regulate natural killer cell development and function. EMBO J 33, 1928-1940.

Chan, A., Hong, D.L., Atzberger, A., Kollnberger, S., Filer, A.D., Buckley, C.D., McMichael, A., Enver, T., and Bowness, P. (2007). CD56bright human NK cells differentiate into CD56dim cells: role of contact with peripheral fibroblasts. J Immunol 179, 89-94.

Chea, S., Possot, C., Perchet, T., Petit, M., Cumano, A., and Golub, R. (2015). CXCR6 Expression Is Important for Retention and Circulation of ILC Precursors. Mediators Inflamm 2015, 368427.

Chiossone, L., Dumas, P.Y., Vienne, M., and Vivier, E. (2018). Natural killer cells and other innate lymphoid cells in cancer. Nat Rev Immunol 18, 671-688.

Chretien, A.S., Devillier, R., Fauriat, C., Orlanducci, F., Harbi, S., Le Roy, A., Rey, J., Bouvier Borg, G., Gautherot, E., Hamel, J.F., et al. (2017a). NKp46 expression on NK cells as a prognostic and predictive biomarker for response to allo-SCT in patients with AML. Oncoimmunology 6, e1307491.

Chretien, A.S., Fauriat, C., Orlanducci, F., Galseran, C., Rey, J., Bouvier Borg, G., Gautherot, E., Granjeaud, S., Hamel-Broza, J.F., Demerle, C., et al. (2017b). Natural Killer Defective Maturation Is Associated with Adverse Clinical Outcome in Patients with Acute Myeloid Leukemia. Front Immunol 8, 573.

Chretien, A.S., Fauriat, C., Orlanducci, F., Rey, J., Borg, G.B., Gautherot, E., Granjeaud, S., Demerle, C., Hamel, J.F., Cerwenka, A., et al. (2017c). NKp30 expression is a prognostic immune biomarker for stratification of patients with intermediate-risk acute myeloid leukemia. Oncotarget 8, 49548-49563.

Cichocki, F., Cooley, S., Davis, Z., DeFor, T.E., Schlums, H., Zhang, B., Brunstein, C.G., Blazar, B.R., Wagner, J., Diamond, D.J., et al. (2016). CD56dimCD57+NKG2C+ NK cell expansion is associated with reduced leukemia relapse after reduced intensity HCT. Leukemia 30, 456-463.

Cichocki, F., Wu, C.Y., Zhang, B., Felices, M., Tesi, B., Tuininga, K., Dougherty, P., Taras, E., Hinderlie, P., Blazar, B.R., et al. (2018). ARID5B regulates metabolic programming in human adaptive NK cells. J Exp Med 215, 2379-2395.

Cooper, M.A., Elliott, J.M., Keyel, P.A., Yang, L., Carrero, J.A., and Yokoyama, W.M. (2009). Cytokine-induced memory-like natural killer cells. Proc Natl Acad Sci U S A 106, 1915-1919.

Cooper, M.A., Fehniger, T.A., and Caligiuri, M.A. (2001). The biology of human natural killer-cell subsets. Trends Immunol 22, 633-640.

Costa-Garcia, M., Ataya, M., Moraru, M., Vilches, C., Lopez-Botet, M., and Muntasell, A. (2019). Human Cytomegalovirus Antigen Presentation by HLA-DR+ NKG2C+ Adaptive NK Cells Specifically Activates Polyfunctional Effector Memory CD4+ T Lymphocytes. Front Immunol 10, 687.

Costello, R.T., Sivori, S., Marcenaro, E., Lafage-Pochitaloff, M., Mozziconacci, M.J., Reviron, D., Gastaut, J.A., Pende, D., Olive, D., and Moretta, A. (2002). Defective expression and function of natural killer cell-triggering receptors in patients with acute myeloid leukemia. Blood 99, 3661-3667.

Crinier, A., Milpied, P., Escaliere, B., Piperoglou, C., Galluso, J., Balsamo, A., Spinelli, L., Cervera-Marzal, I., Ebbo, M., Girard-Madoux, M., et al. (2018). High-Dimensional Single-Cell Analysis Identifies Organ-Specific Signatures and Conserved NK Cell Subsets in Humans and Mice. Immunity 49, 971-986 e975.

Crozat, K., Eidenschenk, C., Jaeger, B.N., Krebs, P., Guia, S., Beutler, B., Vivier, E., and Ugolini, S. (2011). Impact of beta2 integrin deficiency on mouse natural killer cell development and function. Blood 117, 2874-2882.

Dou, Y., Fu, B., Sun, R., Li, W., Hu, W., Tian, Z., and Wei, H. (2015). Influenza vaccine induces intracellular immune memory of human NK cells. PLoS One 10, e0121258.

Dulphy, N., Haas, P., Busson, M., Belhadj, S., Peffault de Latour, R., Robin, M., Carmagnat, M., Loiseau, P., Tamouza, R., Scieux, C., et al. (2008). An unusual CD56(bright) CD16(low) NK cell subset dominates the early posttransplant period following HLA-matched hematopoietic stem cell transplantation. J Immunol 181, 2227-2237.

Durinck, S., Spellman, P.T., Birney, E., and Huber, W. (2009). Mapping identifiers for the integration of genomic datasets with the R/Bioconductor package biomaRt. Nat Protoc 4, 1184-1191.

Falcon, S., and Gentleman, R. (2007). Using GOstats to test gene lists for GO term association. Bioinformatics 23, 257-258.

Fauriat, C., Just-Landi, S., Mallet, F., Arnoulet, C., Sainty, D., Olive, D., and Costello, R.T. (2007). Deficient expression of NCR in NK cells from acute myeloid leukemia: Evolution during leukemia treatment and impact of leukemia cells in NCRdull phenotype induction. Blood 109, 323-330.

Freud, A.G., Yu, J., and Caligiuri, M.A. (2014). Human natural killer cell development in secondary lymphoid tissues. Semin Immunol 26, 132-137.

Guia, S., Fenis, A., Vivier, E., and Narni-Mancinelli, E. (2018). Activating and inhibitory receptors expressed on innate lymphoid cells. Semin Immunopathol 40, 331-341.

Hanna, J., Bechtel, P., Zhai, Y., Youssef, F., McLachlan, K., and Mandelboim, O. (2004). Novel insights on human NK cells' immunological modalities revealed by gene expression profiling. J Immunol 173, 6547-6563.

Huang, L., Zhu, P., Xia, P., and Fan, Z. (2016). WASH has a critical role in NK cell cytotoxicity through Lck-mediated phosphorylation. Cell Death Dis 7, e2301.

Huntington, N.D., Legrand, N., Alves, N.L., Jaron, B., Weijer, K., Plet, A., Corcuff, E., Mortier, E., Jacques, Y., Spits, H., et al. (2009). IL-15 trans-presentation promotes human NK cell development and differentiation in vivo. J Exp Med 206, 25-34.

Jevremovic, D., Billadeau, D.D., Schoon, R.A., Dick, C.J., Irvin, B.J., Zhang, W., Samelson, L.E., Abraham, R.T., and Leibson, P.J. (1999). Cutting edge: a role for the adaptor protein LAT in human NK cell-mediated cytotoxicity. J Immunol 162, 2453-2456.

Khaznadar, Z., Henry, G., Setterblad, N., Agaugue, S., Raffoux, E., Boissel, N., Dombret, H., Toubert, A., and Dulphy, N. (2014). Acute myeloid leukemia impairs natural killer cells through the formation of a deficient cytotoxic immunological synapse. Eur J Immunol 44, 3068-3080.

Leavy, O. (2014). Natural killer cells: RAG keeps natural killers fit. Nat Rev Immunol 14, 716-717.

Lee, J., Zhang, T., Hwang, I., Kim, A., Nitschke, L., Kim, M., Scott, J.M., Kamimura, Y., Lanier, L.L., and Kim, S. (2015). Epigenetic modification and antibody-dependent expansion of memory-like NK cells in human cytomegalovirus-infected individuals. Immunity 42, 431-442.

Lim, A.I., Li, Y., Lopez-Lastra, S., Stadhouders, R., Paul, F., Casrouge, A., Serafini, N., Puel, A., Bustamante, J., Surace, L., et al. (2017). Systemic Human ILC Precursors Provide a Substrate for Tissue ILC Differentiation. Cell 168, 1086-1100 e1010.

Liu, L.L., Landskron, J., Ask, E.H., Enqvist, M., Sohlberg, E., Traherne, J.A., Hammer, Q., Goodridge, J.P., Larsson, S., Jayaraman, J., et al. (2016). Critical Role of CD2 Co-stimulation in Adaptive Natural Killer Cell Responses Revealed in NKG2C-Deficient Humans. Cell Rep 15, 1088-1099.

Liu, L.L., Pfefferle, A., Yi Sheng, V.O., Bjorklund, A.T., Beziat, V., Goodridge, J.P., and Malmberg, K.J. (2015). Harnessing adaptive natural killer cells in cancer immunotherapy. Mol Oncol 9, 1904-1917.

Lopez-Verges, S., Milush, J.M., Schwartz, B.S., Pando, M.J., Jarjoura, J., York, V.A., Houchins, J.P., Miller, S., Kang, S.M., Norris, P.J., et al. (2011). Expansion of a unique

CD57(+)NKG2Chi natural killer cell subset during acute human cytomegalovirus infection. Proc Natl Acad Sci U S A 108, 14725-14732.

Lugthart, G., Melsen, J.E., Vervat, C., van Ostaijen-Ten Dam, M.M., Corver, W.E., Roelen, D.L., van Bergen, J., van Tol, M.J., Lankester, A.C., and Schilham, M.W. (2016). Human Lymphoid Tissues Harbor a Distinct CD69+CXCR6+ NK Cell Population. J Immunol 197, 78-84.

Mace, E.M., and Orange, J.S. (2014). Lytic immune synapse function requires filamentous actin deconstruction by Coronin 1A. Proc Natl Acad Sci U S A 111, 6708-6713.

Melsen, J.E., Lugthart, G., Lankester, A.C., and Schilham, M.W. (2016). Human Circulating and Tissue-Resident CD56(bright) Natural Killer Cell Populations. Front Immunol 7, 262.

Moretta, A., Bottino, C., Vitale, M., Pende, D., Cantoni, C., Mingari, M.C., Biassoni, R., and Moretta, L. (2001). Activating receptors and coreceptors involved in human natural killer cell-mediated cytolysis. Annu Rev Immunol 19, 197-223.

Narni-Mancinelli, E., Ugolini, S., and Vivier, E. (2013). Tuning the threshold of natural killer cell responses. Curr Opin Immunol 25, 53-58.

Pende, D., Spaggiari, G.M., Marcenaro, S., Martini, S., Rivera, P., Capobianco, A., Falco, M., Lanino, E., Pierri, I., Zambello, R., et al. (2005). Analysis of the receptor-ligand interactions in the natural killer-mediated lysis of freshly isolated myeloid or lymphoblastic leukemias: evidence for the involvement of the Poliovirus receptor (CD155) and Nectin-2 (CD112). Blood 105, 2066-2073.

Rabacal, W., Pabbisetty, S.K., Hoek, K.L., Cendron, D., Guo, Y., Maseda, D., and Sebzda, E. (2016). Transcription factor KLF2 regulates homeostatic NK cell proliferation and survival. Proc Natl Acad Sci U S A 113, 5370-5375.

Renoux, V.M., Zriwil, A., Peitzsch, C., Michaelsson, J., Friberg, D., Soneji, S., and Sitnicka, E. (2015). Identification of a Human Natural Killer Cell Lineage-Restricted Progenitor in Fetal and Adult Tissues. Immunity 43, 394-407.

Sanchez-Correa, B., Gayoso, I., Bergua, J.M., Casado, J.G., Morgado, S., Solana, R., and Tarazona, R. (2012). Decreased expression of DNAM-1 on NK cells from acute myeloid leukemia patients. Immunol Cell Biol 90, 109-115.

Sasanuma, H., Tatsuno, A., Hidano, S., Ohshima, K., Matsuzaki, Y., Hayashi, K., Lowell, C.A., Kitamura, D., and Goitsuka, R. (2006). Dual function for the adaptor MIST in IFN-gamma production by NK and CD4+NKT cells regulated by the Src kinase Fgr. Blood 107, 3647-3655.

Satija, R., Farrell, J.A., Gennert, D., Schier, A.F., and Regev, A. (2015). Spatial reconstruction of single-cell gene expression data. Nat Biotechnol 33, 495-502.

Schlums, H., Cichocki, F., Tesi, B., Theorell, J., Beziat, V., Holmes, T.D., Han, H., Chiang, S.C., Foley, B., Mattsson, K., et al. (2015). Cytomegalovirus infection drives adaptive epigenetic diversification of NK cells with altered signaling and effector function. Immunity 42, 443-456.

Scoville, S.D., Nalin, A.P., Chen, L., Chen, L., Zhang, M.H., McConnell, K., Beceiro Casas, S., Ernst, G., Traboulsi, A.A., Hashi, N., et al. (2018). Human AML activates the aryl hydrocarbon receptor pathway to impair NK cell development and function. Blood 132, 1792-1804.

Short, N.J., Konopleva, M., Kadia, T.M., Borthakur, G., Ravandi, F., DiNardo, C.D., and Daver, N. (2020). Advances in the Treatment of Acute Myeloid Leukemia: New Drugs and New Challenges. Cancer Discov 10, 506-525.

Spits, H., Artis, D., Colonna, M., Diefenbach, A., Di Santo, J.P., Eberl, G., Koyasu, S., Locksley, R.M., McKenzie, A.N., Mebius, R.E., et al. (2013). Innate lymphoid cells--a proposal for uniform nomenclature. Nat Rev Immunol 13, 145-149.

Stringaris, K., Sekine, T., Khoder, A., Alsuliman, A., Razzaghi, B., Sargeant, R., Pavlu, J., Brisley, G., de Lavallade, H., Sarvaria, A., et al. (2014). Leukemia-induced phenotypic and functional defects in natural killer cells predict failure to achieve remission in acute myeloid leukemia. Haematologica 99, 836-847.

Stumpo, D.J., Broxmeyer, H.E., Ward, T., Cooper, S., Hangoc, G., Chung, Y.J., Shelley, W.C., Richfield, E.K., Ray, M.K., Yoder, M.C., et al. (2009). Targeted disruption of Zfp36l2, encoding a CCCH tandem zinc finger RNA-binding protein, results in defective hematopoiesis. Blood 114, 2401-2410.

Tesi, B., Schlums, H., Cichocki, F., and Bryceson, Y.T. (2016). Epigenetic Regulation of Adaptive NK Cell Diversification. Trends Immunol 37, 451-461.

Trapnell, C., Cacchiarelli, D., Grimsby, J., Pokharel, P., Li, S., Morse, M., Lennon, N.J., Livak, K.J., Mikkelsen, T.S., and Rinn, J.L. (2014). The dynamics and regulators of cell fate decisions are revealed by pseudotemporal ordering of single cells. Nat Biotechnol 32, 381-386.

van Helden, M.J., Goossens, S., Daussy, C., Mathieu, A.L., Faure, F., Marcais, A., Vandamme, N., Farla, N., Mayol, K., Viel, S., et al. (2015). Terminal NK cell maturation is controlled by concerted actions of T-bet and Zeb2 and is essential for melanoma rejection. J Exp Med 212, 2015-2025.

Viant, C., Fenis, A., Chicanne, G., Payrastre, B., Ugolini, S., and Vivier, E. (2014). SHP-1-mediated inhibitory signals promote responsiveness and anti-tumour functions of natural killer cells. Nat Commun 5, 5108.

Vivier, E., Raulet, D.H., Moretta, A., Caligiuri, M.A., Zitvogel, L., Lanier, L.L., Yokoyama, W.M., and Ugolini, S. (2011). Innate or adaptive immunity? The example of natural killer cells. Science 331, 44-49.

Walzer, T., Chiossone, L., Chaix, J., Calver, A., Carozzo, C., Garrigue-Antar, L., Jacques, Y., Baratin, M., Tomasello, E., and Vivier, E. (2007a). Natural killer cell trafficking in vivo requires a dedicated sphingosine 1-phosphate receptor. Nat Immunol 8, 1337-1344.

Walzer, T., Jaeger, S., Chaix, J., and Vivier, E. (2007b). Natural killer cells: from CD3(-)NKp46(+) to post-genomics meta-analyses. Curr Opin Immunol 19, 365-372.

Wilton, K.M., Overlee, B.L., and Billadeau, D.D. (2019). NKG2D-DAP10 signaling recruits EVL to the cytotoxic synapse to generate F-actin and promote NK cell cytotoxicity. J Cell Sci 133.

Witalisz-Siepracka, A., Klein, K., Prinz, D., Leidenfrost, N., Schabbauer, G., Dohnal, A., and Sexl, V. (2018). Loss of JAK1 Drives Innate Immune Deficiency. Front Immunol 9, 3108.

Yang, C., Siebert, J.R., Burns, R., Gerbec, Z.J., Bonacci, B., Rymaszewski, A., Rau, M., Riese, M.J., Rao, S., Carlson, K.S., et al. (2019). Heterogeneity of human bone marrow and blood natural killer cells defined by single-cell transcriptome. Nat Commun 10, 3931.

Yu, J., Freud, A.G., and Caligiuri, M.A. (2013). Location and cellular stages of natural killer cell development. Trends Immunol 34, 573-582.

Yu, J., Mitsui, T., Wei, M., Mao, H., Butchar, J.P., Shah, M.V., Zhang, J., Mishra, A., Alvarez-Breckenridge, C., Liu, X., et al. (2011). NKp46 identifies an NKT cell subset susceptible to leukemic transformation in mouse and human. J Clin Invest 121, 1456-1470.

Zhang, L., Prak, L., Rayon-Estrada, V., Thiru, P., Flygare, J., Lim, B., and Lodish, H.F. (2013). ZFP36L2 is required for self-renewal of early burst-forming unit erythroid progenitors. Nature 499, 92-96.

Zheng, G.X., Terry, J.M., Belgrader, P., Ryvkin, P., Bent, Z.W., Wilson, R., Ziraldo, S.B., Wheeler, T.D., McDermott, G.P., Zhu, J., et al. (2017). Massively parallel digital transcriptional profiling of single cells. Nat Commun 8, 14049.

CLAIMS:

1. A method of predicting the survival time of a patient suffering from an acute myeloid leukemia (AML) comprising determining the level of CD160 in a sample obtained from the patient wherein said level correlates with the patient's survival time.

2. The method of claim 1 wherein the sample is a blood sample.

3. The method of claim 1 wherein the sample is a bone marrow sample.

4. The method of claim 1 wherein the level of CD160 is determined at the protein level, in particular by contacting the sample with at least one selective binding agent capable of selectively interacting with CD160.

5. The method of claim 4 wherein the binding agent is an antibody.

6. The method of claim 4 wherein the level of CD160 is determined by immunohistochemistry.

7. The method of claim 1 wherein the level of CD160 is determined at nucleic acid level, in particular by determining the quantity of mRNA encoding for CD160.

8. The method of claim 7 wherein said expression is determined by nucleic acid array, PCR, qPCR, RT-qPCR, or RNAseq.

9. The method of claim 1 wherein the level of CD160 is expressed as measurement of the expression intensity of the marker (e.g. protein and/or mRNA) by NK cells (e.g. mean fluorescence intensity MFI) or as measurement of the amount of NK cells that express CD160 (e.g. protein and/or mRNA) in a sample (e.g. frequencies (e.g. %) of CD160+ NK cells and density of C160+ NK cells).

10. The method of claim 9 wherein a panel of binding partners that are specific for the cell surface markers CD3, CD56 and CD160 is used for determining the level of CD160 in NK cells.

11. The method of claim 9 wherein the level of C160 in NK cells is determined by a flow cytometric method.

12. The method of claim 9 wherein the level of C160 in NK cells is determined by single cell RNA sequencing.

13. The method of claim 1 wherein the lower is the level of CD160, the higher is the probability that the patient will have a short survival time.

14. The method of claim 1 that comprises the steps of i) determining the level of CD160 in the sample obtained from the patient, ii) comparing the level determined at step i) with a predetermined reference value and iii) concluding that the patient has a good prognosis when the level determined at step i) is higher than the predetermined reference value or concluding that the patient has a poor prognosis when the level determined at step i) is lower than the predetermined reference value.

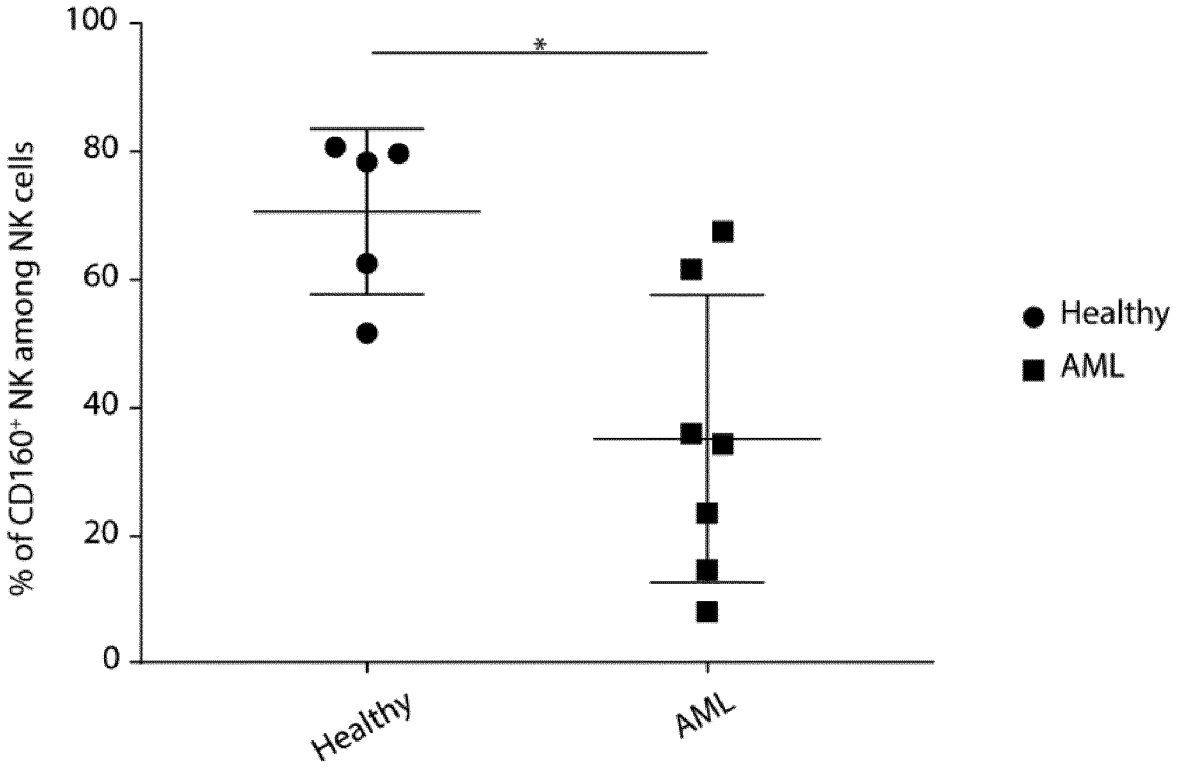

Figure 1

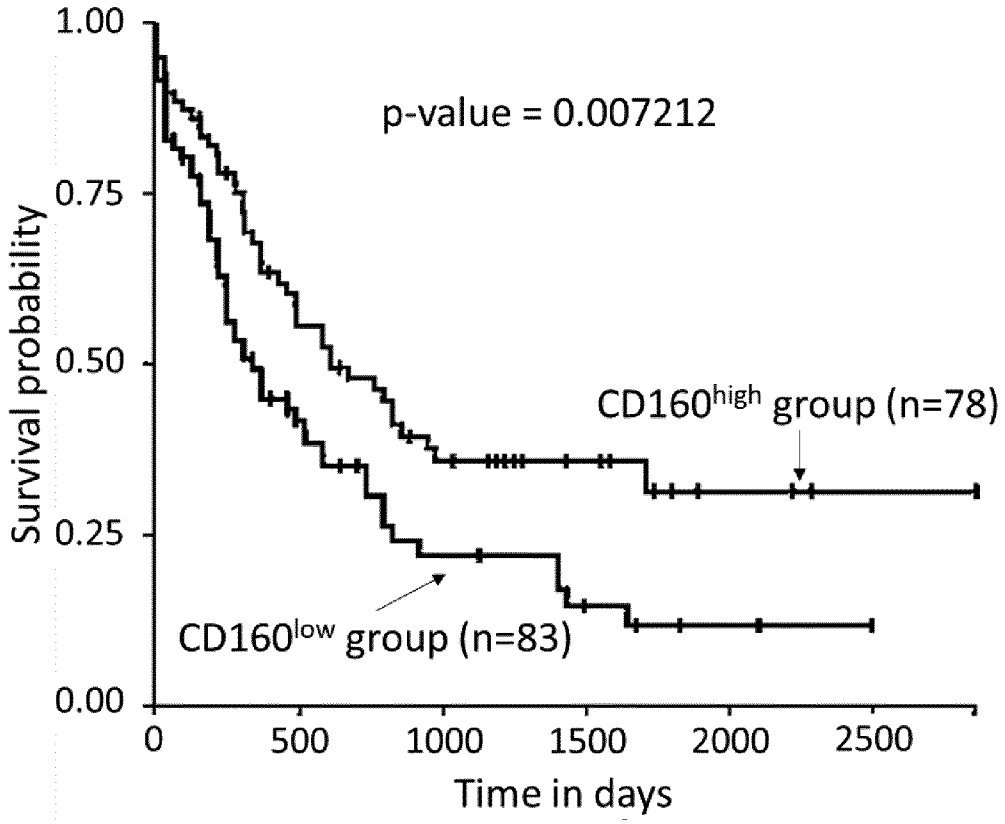

Figure 2

INTERNATIONAL SEARCH REPORT

International application No
PCT/EP2021/069529

A. CLASSIFICATION OF SUBJECT MATTER
INV. G01N33/574
ADD.

According to International Patent Classification (IPC) or to both national classification and IPC

B. FIELDS SEARCHED

Minimum documentation searched (classification system followed by classification symbols)
G01N

Documentation searched other than minimum documentation to the extent that such documents are included in the fields searched

Electronic data base consulted during the international search (name of data base and, where practicable, search terms used)

EPO-Internal, BIOSIS, EMBASE

C. DOCUMENTS CONSIDERED TO BE RELEVANT

Category*	Citation of document, with indication, where appropriate, of the relevant passages	Relevant to claim No.
A	WO 2018/162404 A1 (INST NAT SANTE RECH MED [FR]; UNIV DAIX MARSEILLE [FR] ET AL.) 13 September 2018 (2018-09-13) claim 1	1-14
A	WO 2018/146239 A1 (INST NAT SANTE RECH MED [FR]; UNIV DAIX MARSEILLE [FR] ET AL.) 16 August 2018 (2018-08-16) claim 1	1-14

☐ Further documents are listed in the continuation of Box C.

☒ See patent family annex.

* Special categories of cited documents :

"A" document defining the general state of the art which is not considered to be of particular relevance

"E" earlier application or patent but published on or after the international filing date

"L" document which may throw doubts on priority claim(s) or which is cited to establish the publication date of another citation or other special reason (as specified)

"O" document referring to an oral disclosure, use, exhibition or other means

"P" document published prior to the international filing date but later than the priority date claimed

"T" later document published after the international filing date or priority date and not in conflict with the application but cited to understand the principle or theory underlying the invention

"X" document of particular relevance; the claimed invention cannot be considered novel or cannot be considered to involve an inventive step when the document is taken alone

"Y" document of particular relevance; the claimed invention cannot be considered to involve an inventive step when the document is combined with one or more other such documents, such combination being obvious to a person skilled in the art

"&" document member of the same patent family

Date of the actual completion of the international search	Date of mailing of the international search report
15 September 2021	04/10/2021

Name and mailing address of the ISA/	Authorized officer
European Patent Office, P.B. 5818 Patentlaan 2 NL - 2280 HV Rijswijk Tel. (+31-70) 340-2040, Fax: (+31-70) 340-3016	Rosin, Oliver

1

INTERNATIONAL SEARCH REPORT

Information on patent family members

International application No
PCT/EP2021/069529

Patent document cited in search report	Publication date	Patent family member(s)	Publication date
WO 2018162404 A1	13-09-2018	NONE	
WO 2018146239 A1	16-08-2018	NONE	